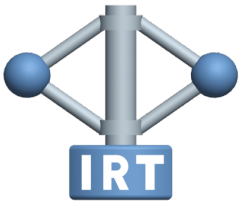

Jaco Zingerle, BSc

Validation of Comfort based HVAC Control

Master's Thesis
at
Technical University of Graz
in
Electrical engineering

In cooperation with
VIRTUAL VEHICLE Research GmbH

Supervisor
Assoc.Prof. Dipl.-Ing. Dr.techn. Markus Reichhartinger

20.01.2021

Statutory Declaration

I declare that I have authored this thesis independently, that I have not used other than the declared sources/resources, and that I have explicitly marked all material which has been quoted either literally or by content from the used sources.

....

date signature

Abstract

The HVAC (Heating, Ventilation and Air Conditioning)-system is an increasingly important part of every passenger vehicle nowadays. An adequate temperature in the car is crucial for the passenger's comfort.

The main goal is to reach a comfortable temperature for every part of the body, which is a challenging task that has yet to be achieved. Most new cars nowadays have a temperature control for the car compartment, controls for the temperature of individual parts of the body, controls for the airflow and the direction of the air via servo motors. Even steering wheel and seat heating is state of the art by now.

Adaptive HVAC controls are often used to reach a comfortable temperature for the cabin. With a flow and temperature model of the car interior it is possible to determine what temperature and airflow needs to enter the car from what outlet to reach a desired temperature in a specific part of the car compartment. Of course, the solution is limited by the number and position of the air outlets and the possible airflow and temperature that can be reached at those.

Even with all the existing HVAC controls, the driver still has the possibility to intervene manually and change the airflow and temperature at the inlets if he feels uncomfortable. Target of this project is to predict comfortable inlet conditions using a driver and cabin model, such that no intervention is required. If the driver model is not good enough, the algorithm has to learn and adapt.

The focus of this thesis is to control the HVAC system of the car in a way, such that the temperature and airflow at every outlet gets as close as possible to the specification given by the adaptation algorithm.

Kurzfassung

Die Klimaanlage in Fahrzeugen nimmt heutzutage immer mehr an Bedeutung zu. Eine angenehme Temperatur im Innenraum ist entscheidend für das Wohlbefinden der Insassen.

Dabei ist das Erreichen einer angenehmen Temperatur für jede Körperregion das Ziel. Das ist eine herausfordernde Aufgabe, die es noch bewältigen gilt. Die meisten modernen Autos verfügen über Temperaturregelungen für den Innenraum, Regelungen für einzelne Köperbereiche, Volumenstromregelungen und Regelungen der Einströmrichtung über Servomotoren. Sogar Lenkrad- und Sitzheizung gelten heutzutage als Standard.

Adaptive Klimaregelungen sind eine beliebte Methode um angenehme Temperaturen im Innenraum zu erreichen. Ein Temperatur- und Strömungsmodell des Inneraums ermöglicht es zu bestimmen, welche Temperatur mit welcher Strömunggeschwindigkeit von welchem Einlass einströmen muss, um eine bestimmte Temperatur in einer Körperregion zu erreichen. Natürlich ist diese Lösung sowohl von der Anzahl und Lage der Einströmer, als auch von den physikalisch möglichen Strömungsgeschwindigkeiten und Temperaturen, die an diesen Auslässen erreicht werden können, begrenzt.

Sogar mit den ganzen Klimaregelungen, die es gibt, hat der Fahrer immer noch die Möglichkeit manuell einzugreifen, um die Einströmbedingugnen zu ändern, falls dieser sich unwohl fühlt. Ziel dieses Projekts ist es, angenehme Einströmbedingugnen mittels eines Fahrer und Kabinenmodells zu prädizieren, sodass kein eingreifen notwendig ist. Falls das Modell nicht ausreichend gut ist, soll der Algorithmus dazulernen und sich anpassen.

Der Fokus dieser Arbeit liegt darin, die Klimaanlage so zu regeln, sodass die Einströmbedingungen so nah wie möglich an den Referenzgrößen des Algorithmus heranreichen.

Contents

List of Figures

Symbols and Acronyms

HVAC	Heating, Ventilation and Air Conditioning
CFD	Computational Fluid Dynamics
PPM	Pulse Pause Modulation
$\dot{V}$	volume flow in m^3/s
Δp	pressure loss in kg/m^2
ρ	density in kg/m^3
T_a	air temperature in $°C$
T_w	water temperature in $°C$
$T_{HVAC,in}$	temperature of the air entering the HVAC in $°C$
$T_{car,in}$	temperature of the air entering the car in $°C$
τ_s	time constant of the temperature sensor in s
τ_{TC}	time constant of the thermocouple in s
τ_m	time constants of the motor heating in s
K_m	motor heating gain in $°C$
P_m	blower motor power in W
$G_m(s)$	blower motor transfer function
$c_{p,a}$	specific isobar heat capacity of the air in $J/kg°C$
c_h	heat capacity of the electric heater in $J/kg°C$
R_m	airflow resistance of the middle valve in kg/m^7
R_f	airflow resistance of the feet valve in kg/m^7
R_w	airflow resistance of the windshield valve in kg/m^7
$m_{a,h}$	mass of the air inside the heater in kg
m_h	mass of the heater in kg
k_h	heat transfer coefficient in $W/m^2 \circ C$
A_h	area of the heat transfer between the heater and the air in m^2
k_p	constant to describe how much energy is lost in the wire
a	opening of the temperature valve in percent
w	opening of windshield valve in percent
m	opening of middle console valve in percent
f	opening of feet valve in percent
A_m	vector of the measured outlet areas in cm^2
A_c	vector of the calculated outlet areas in cm^2

1 Introduction

The first part of the introduction gives a brief overview of the existing automotive HVAC technologies and an outlook in what direction the research is leading to. The second part gives an overview of how the adaptation algorithm used in this project works. The final part of the introduction is about the tasks to accomplish and the goals to reach.

Section 2 explains the single components of the system and how they are connected to each other. Section 3 gives an overview of the required physical basics to understand the modeling approach used in Section 4 and the control strategies used in Section 5. Section 6 presents the first results of the system using probands. The summary of this work and an outlook is given in Section 7.

1.1 Automotive HVAC Technologies

According to [8], the fast improvement of data acquisition and measurement systems in addition to the faster processing units and real-time data evaluation systems in the past years opened the possibility to add more and better sensors to automotive vehicles, allowing a better thermal resolution of the car interior. Better simulation based control strategies could be designed due to the improvements in numerical simulation and processing power.

Those changes allowed the use of advanced and more automated control techniques in automotive HVAC control. Multiple new test applications could be built to test different environments and consider more possibilities, like hot roads, sunlight exposure and ambient temperatures [8], [2]. Also the amount of passengers inside the car can be estimated using seat occupancy detectors [5]. The number of passengers inside the car can be an important parameter, since every passenger radiates heat. Also learning algorithms set to remember different environmental conditions and learn from the driver input are used [4].

Improvements in servo motors made fully automated valve control in different areas possible. The valves can be used to control the airflow in different parts of the car, but also automating the outflow direction of the air, like in the new HVAC system of Tesla [10].

Dividing the car into multiple zones has always been a common strategy for temperature control in vehicles. Being able to control the temperature of different areas of the car interior thanks to the increased number of sensors gives the possibility of a higher comfort for the passengers. A simple form of this strategy is used in this project.

1.2 Adaptation Loop

In order to explain the idea used within this thesis, it is important to understand how an adaptive comfort control works. A general description of the closed loop system is shown in Figure 1.

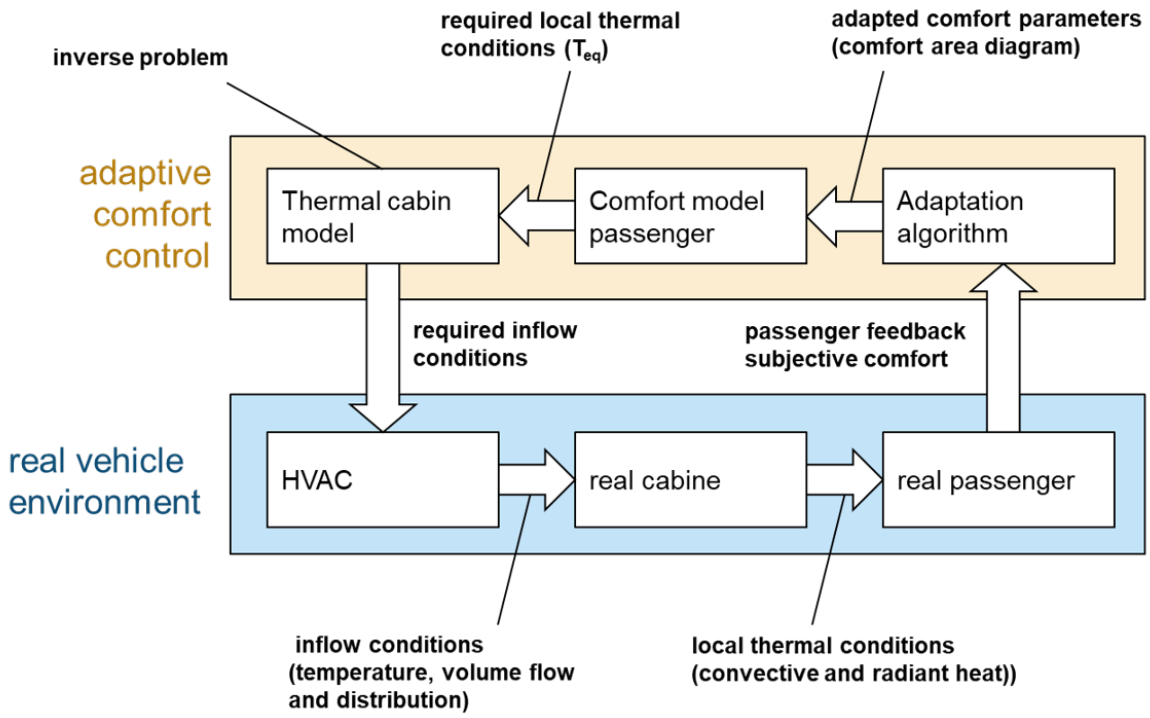

Figure 1: Closed loop system of the adaptive comfort control and the vehicle environment [9].

The system is composed by the adaptive comfort control and the real vehicle environment.

Starting with the HVAC at the bottom left, which gets the required inflow conditions from the adaptive comfort model. In this specific case, the inflow conditions are the temperature, the mass flow and its distribution on the inlets. The main focus of this work is on the HVAC-system and how to satisfy those conditions.

Continuing the cycle counter clockwise, the inflow conditions enter the real cabin. The result are local thermal conditions for the passenger. The passenger can give feedback on his/her subjective comfort. In this case, the comfort feedback consists of three variables, which are divided in cold, slightly cold, comfortable, warm and too warm for the comfort areas of head, torso and feet.

The adaptation algorithm calculates new comfort parameters, based on the passenger feedback. Figure 2 shows the idea of the algorithm for a few iterations.

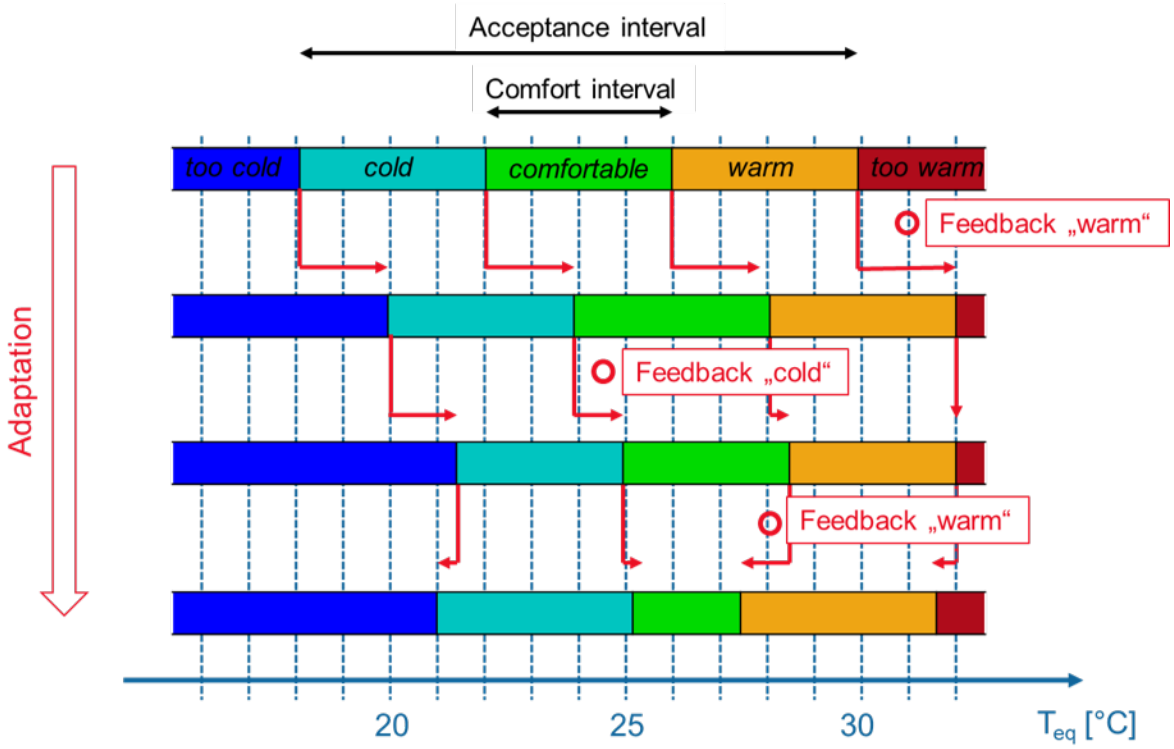

Figure 2: Adaptation of the algorithm for every feedback [9]

Since every passenger has a different feeling of comfort, the right comfort zone has to be found. The size and position of the comfort interval changes based on the feedback of the passenger. The new comfort parameters are handed over to the comfort model of the passenger, which calculates the required thermal conditions, so that the passenger feels comfortable. Those conditions enter the thermal cabin model, from which an inverse problem is solved, the required thermal conditions are known, the required inflow conditions needed to satisfy those are calculated.

For the purpose of a better understanding, the model of the car compartment is shown in Figure 3 and a thermal simulation in Figure 4.

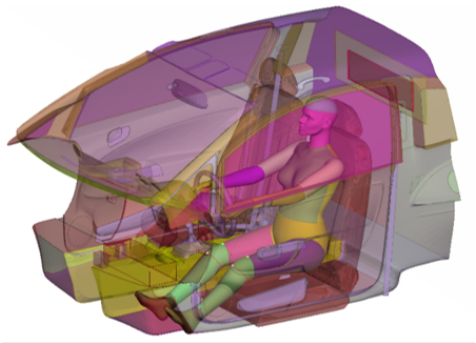

Figure 3: Opel Corsa 3D CAD model [9]

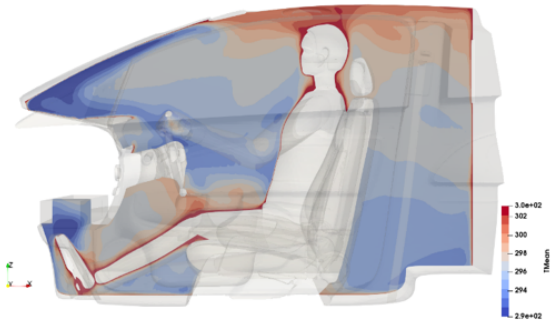

Figure 4: Thermal CFD simulation of the cabin [9]

1.3 Tasks and Goals

The main focus of this work is related to the lower part of the system shown is Figure 1, which is, the real vehicle environment. The inflow conditions should be reached in less than one minute for an effective comfort control.

A control for the total volume flow and the temperature has to be developed.

A control strategy for the airflow distribution has to be developed. However, it is not possible to measure the mass flow on the single inlets, because there is no room for volume flow sensors in the given setup.

At last, but not least, the system has to be tested on probands and the results have to be evaluated for future improvements.

2 System Description

The car used for the project is an Opel Corsa. The car has been halved, since it is being used as a driving simulator. It is useful to use a driving simulator for this project, since the participants have the possibility to run trough simulated driving scenarios, since the movements while driving also produce heat. The car is placed on four pneumatic pistons to allow a feeling of motion for the driver. A picture of the car is shown in Figure 5.

Figure 5: Driving simulator used for the project.

The piping from the back to the front of the car has been applied to allow air circulation. An air circulation cycle enables a much lower heating or cooling capacity, because the amount of air in the system is limited. The core component of the HVAC-System is the HVAC-box, a picture of the HVAC-Box of the Opel Corsa is shown in Figure 6. The acceleration of the air, the cooling or heating and the air distribution all takes place inside the HVAC-Box.

Figure 6: Photo of the HVAC-box with mounted servo motors [7]

The mounted servo motors are used to control the position of the valves. A schematic representation of the system with all the present components is shown in Figure 7. The blue line represents the cooled water from the external water chiller and the red line represents the electric current flowing trough the heater and the blower motor.

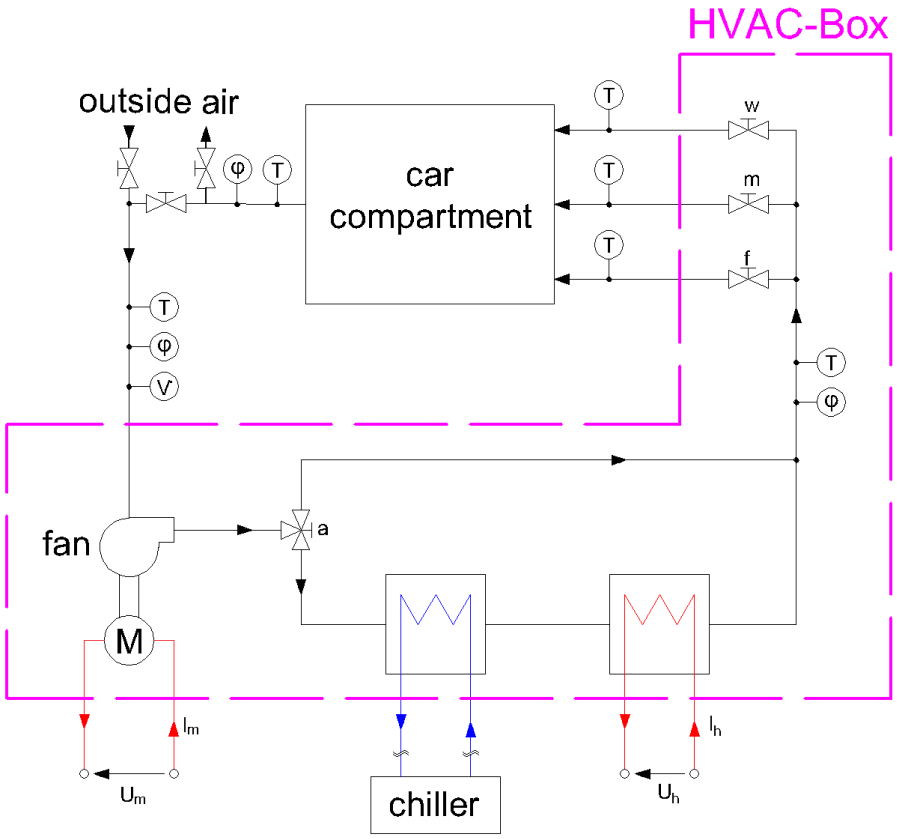

Figure 7: Representation of the whole system.

Starting at the bottom left of Figure 7, there is the blower motor that sucks in the mix of recirculating and outside air. The humidity, the temperature and the volume flow of the air are measured before the blower motor.

The valve a on the right of the blower motor in Figure 7 is used as a bypass to control how much air flows trough the heater and cooler core. Since the car doesn't have a refrigeration cycle anymore, an external chiller was connected. The water flowing from the external water chiller through the cooler core and back into the chiller is pictured in blue. The heater is an electric heater, the temperature can be controlled with the voltage U_h and the current I_h drawn in red.

The air is then again merged and the temperature and humidity is measured. The airflow is then split into three paths by the valves f, flowing to the feet, the valve m, flowing to the middle control panel and the valve w, that flows to the windshield. The valves on each path are used to control the airflow. The temperature is measured at every outlet.

The air proceeds into the car compartment. At the back of the cabin the temperature and humidity are again measured. The valves at the top left of the picture are used to control how much outside air is mixed with the recirculating air.

2.1 Blower Motor

The fan is a radial blower. The motor is a DC-motor. A picture of the blower motor is shown in Figure 8.

Figure 8: Photo of the blower motor.

The current of the blower motor at $15V$ and steady state was measured. The result of the measurement was a $20A$ current, the maximum steady state power of the blower motor therefore equals about $300W$. A PWM DC power controller is used to control the blower motor.

2.2 External Water Chiller and Cooler Core

The external water chiller is placed outside the room. The cooled water is guided inside the room through the window, flows through the cooler core and is then again guided outside the room back into the chiller. A picture of the chiller is shown in Figure 9, a picture of the cooler core in Figure 10.

Figure 9: Photo of the external water chiller.

Figure 10: Photo of the cooler core.

The chiller has a two setpoint temperature control. The resulting hysteresis causes an oscillation of the water temperature.

2.3 Electric Air Heater

The electric heater is used to heat the air. It has three connectors. A picture of the heater is shown in Figure 11.

Figure 11: Photo of the electric heater.

Since there is no data available on the heater, the temperature was measured for different voltages and currents.

A voltage was applied to the gray and the green connector of the electric heater separately. While the temperature of the heater was increasing, the current and voltage for the specific temperatures was measured. Using the measured data the resistance of the coils depending on the temperature can be computed. The result is shown in Figure 6.

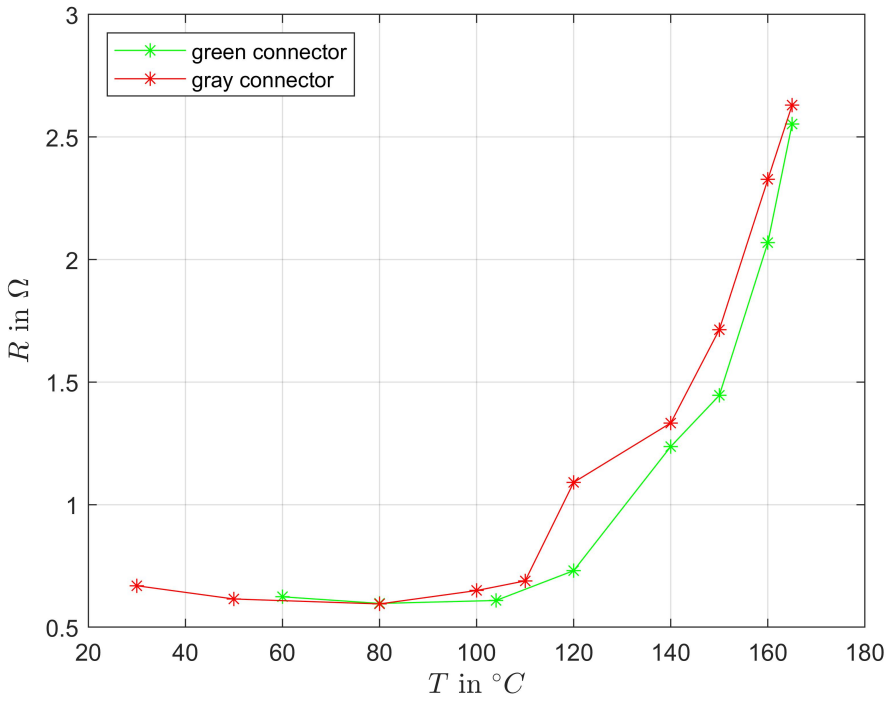

Figure 12: Resistance as function of the temperature of the electric heater coils.

It is to note, that the measurements have a low accuracy, since only the basic characteristics of the heater are required here. The electric heater has a positive temperature coefficient, meaning that its resistance increases with the temperature. It is assumed that the blue coil of the electric heater shows similar characteristics. The measurement data shows that the temperature is limited at approximately 165°C for the given voltage. The electric heater consumes a maximum of about $240W$ at low temperatures. The same power controller used for the blower motor can be used for the electric heater.

2.4 Sensors

The volume flow sensor uses differential pressure, the volume flow can then be calculated using the formula from the pipe data sheet given by the manufacturer as

$$\dot{V} = C\sqrt{\Delta p}\sqrt{\frac{1.2}{\rho}},$$

where in this case, ρ is the air density, Δp is the differential pressure and C is a pipe specific parameter given as $0.0097 m^3/s$ for the used pipe. The nonlinear function of the sensor is shown in Figure 13.

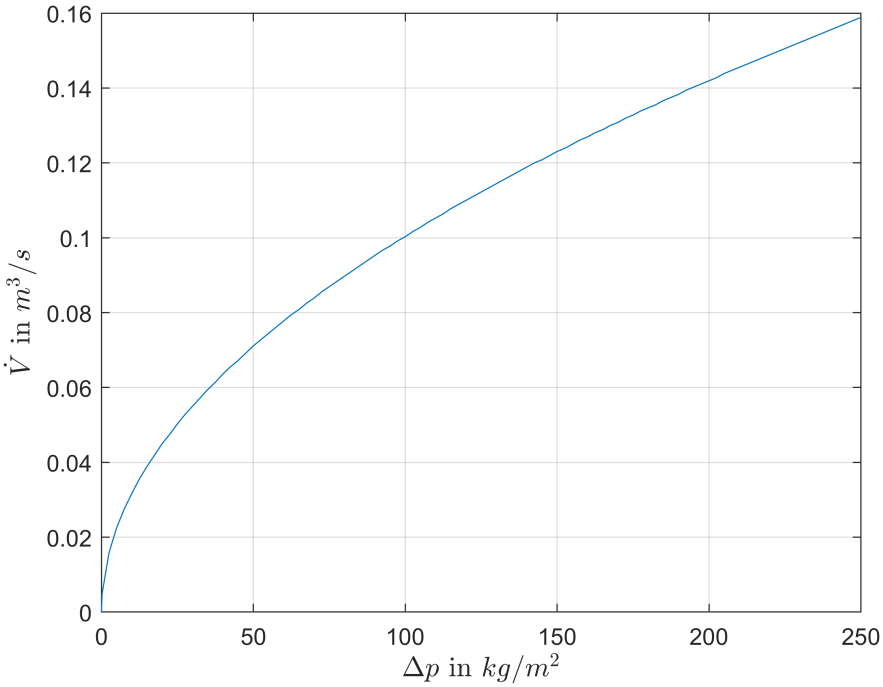

Figure 13: Volume flow as function of the pressure loss for the volume flow sensor.

A temperature sensor with large time constant was placed in the HVAC-Box. The reason for using this sensor is that a fast sensor might oscillate due to the cold and warm air being mixed. To find the dynamics of the sensor and of the air mixing, the chiller was turned on and the temperature valve was set to let all the air bypass the cooler core. At time $t = 0$ the temperature valve was set to let all the air flow trough the cooler core. The time constant of the sensor and the air mixing was estimated as $\tau_s = 100.4$ using minimization in the least squares sense. The comparison between measurement and simulation with the estimated time constant τ_s is shown in Figure 14.

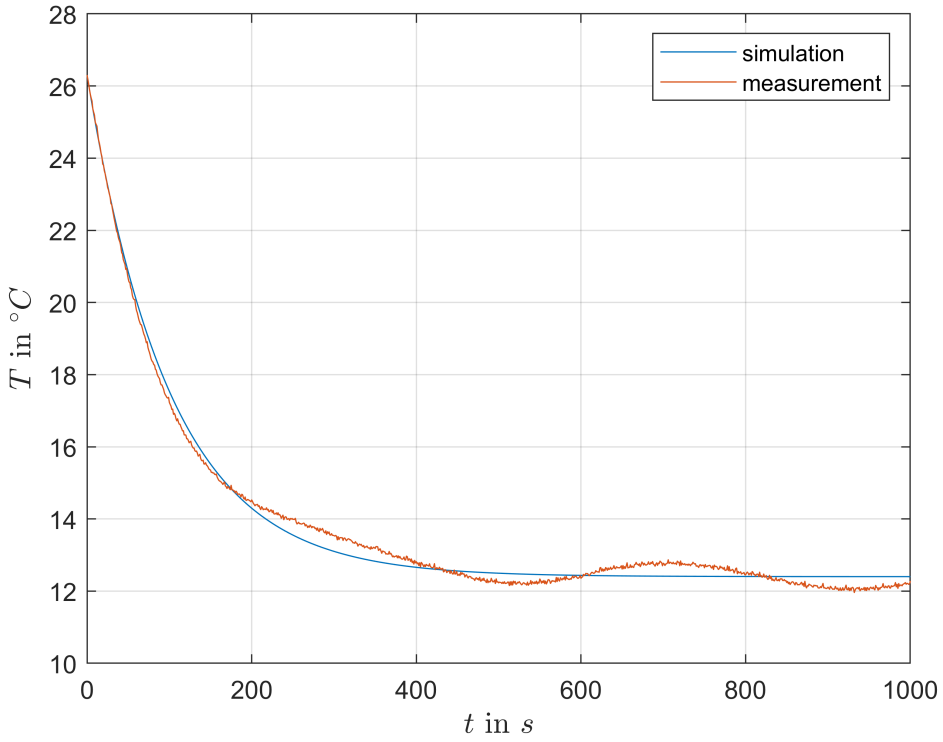

Figure 14: Measured and simulated temperature sensor dynamics.

No fast variations of the temperature are expected for the other two sensors measuring the temperature and the humidity placed at the back of the car and before the HVAC-box, for this reason their dynamics can be neglected.

All other temperature sensors are K-type thermocouples.

2.5 Valves

The four valves shown in Figure 7 have the following function:

- Valve m: depending on the valve angle m, the amount of air flowing to the middle console and the side window outlets can be adjusted.
- Valve f: depending on the valve angle f, the amount of air flowing to the feet can be adjusted.
- Valve w: depending on the valve angle w, the amount of air flowing to the windshield and defrost outlets can be adjusted.
- Valve a: depending on the valve angle a, the amount of air bypassing the electric heater and the cooler core is adjusted.

Every valve needs to be controlled separately, therefore a servo motor for every valve was mounted. The servo motors are controlled using a Pulse Position Modulation

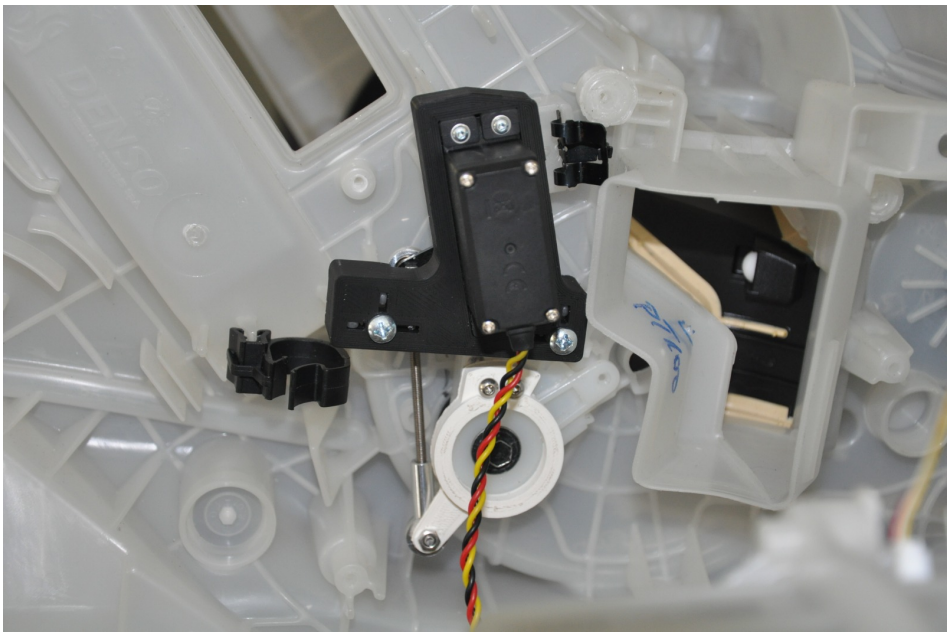

Figure 15: Mounting of a servo motor on the HVAC-Box [7].

(PPM)-signal. To give a better idea, a photo of a servo motor and its mounting is shown in Figure 15. The maximum and minimum angle possible for every valve was measured. The result is shown in Table 1.

servo motor	PPM duty cycle	PPM duty cycle
	open	closed
a	0.1	0.055
w	0.06	0.1
m	0.07	0.04
f	0.1	0.075

Table 1: Limit measurements for the servo motors. For the temperature valve a, open means all the air flows trough the heater or cooler core.

It is important to note, that the angle of the servo motors are not linear to the valve angles due to the way they were mounted. The angles a, f, m and w referred to in the rest of this work are the angles of the servo motor, not the angles of the valves. For more information about the servo motor choice and their mounting can be found in [7].

3 Physical Basics and Existing Literature

The required basics of thermodynamics and fluid mechanics for the physical model are presented in this chapter.

3.1 Energy and Mass Conservation

The information of this section is based on [1]. In thermodynamics typically it is distinguished between isolated, closed and open systems.

Isolated systems don't allow any kind of energy or mass to pass the system boundary. Closed systems only allow energy, but not mass to pass the system boundary. Open systems on the other hand allow both, mass and energy to pass the system boundary.

Starting with the assumptions and the principles of energy conservation, the first law of thermodynamics for closed systems, i.e.,

$$\Delta U = Q - W, \tag{1}$$

states that the change of the internal energy ΔU in the system is equal to the difference of energy that crosses the system boundary as heat Q and work W. The internal energy U is defined as

$$U = E - E_{kin} - E_{pot}.$$

That means that the work in equation (1) doesn't include the potential and kinetic energy acting on the system as a whole, since they do not pass the system's boundary. For future derivations the specific internal energy u of a material is defined as

$$u = \frac{U}{m},$$

where m is the mass of the system. The heat Q is a form of energy driven by the temperature difference in two adjacent materials. The heat transfer $\dot{Q}$ from system A to system B, with the temperatures $T_B > T_A$ can be described with the formula

$$\dot{Q} = kA(T_B - T_A), \tag{2}$$

where k is the heat transfer coefficient and A is the area connecting systems A and B. The heat transfer coefficient depends mainly on the materials involved in the heat transfer process. The borderline case $k \to 0$ represents a so called "adiabatic wall", a wall that doesn't allow any heat transfer. Such a wall doesn't exist in reality but is often used for modeling purposes when the heat transfer is neglectable.

To describe an open system, the mass flow has to be added. Therefore the principle of mass conservation is introduced. The change of mass in a system is defined as

$$\frac{dm}{dt} = \sum_{in} \dot{m}_i(t) - \sum_{out} \dot{m}_o(t)$$

where $\dot{m}_i(t)$ and $\dot{m}_o(t)$ are the time dependent mass flows entering and leaving the system.

Obviously, the mass flow brings energy into or takes energy away from the system. To describe the energy of a mass flow entering the system, the specific energy is defined as

$$e = \frac{E}{m}.$$

The specific energy of a fluid passing the system boundary can be described as

$$e = u + \frac{c^2}{2} + gz,$$

where u equals the specific internal energy, $c^2/2$ is the specific kinetic energy with flow speed c and gz is the specific potential energy with the gravitational acceleration g and the height z.

The mass flow also entails pressure-volume work, which falls in the category of work W from equation (1). This pressure-volume work W_V can be described as

$$W_V(t) = pv\dot{m},$$

with p, v and $\dot{m}$ being pressure, specific volume and mass flow. With the results from above it is now possible to formulate the general power equation

$$\frac{dE}{dt} = \dot{Q} + P + \dot{m}(u + pv + \frac{c^2}{2} + gz). \tag{3}$$

It is not specifically stated that all the quantities from equation (3) are time dependent with g being the only exception.

Another important quantity is the energy stored in a material. The heat capacity C with the unit Joule per Kelvin describes the ability of a material to store heat. The heat capacity is an extensive property of a system. The specific heat capacity on the other hand is the intensive equivalent and is defined as:

$$c = \frac{C}{m}.$$

The specific heat capacity is used to describe thermodynamic systems since it is known for the most common materials. The change of thermal energy stored in a material can be described as

$$\frac{dE}{dt} = mc\frac{dT}{dt}, \tag{4}$$

with m and c being the mass and the specific heat capacity of the material.

3.2 Airflow Dynamics

According to [6], the pressure loss Δp in a pipe can be described by the formula

$$\Delta p = \zeta \frac{\rho}{2} \frac{\dot{V}^2}{A^2},$$

where ζ, ρ $\dot{V}$ and A are the pipe friction coefficient, the density of the material flowing trough, the volume flow and the area of the pipe respectively. By assuming constant density and area, the formula can be simplified as

$$\Delta p = R\dot{V}^2,$$

where R is the flow resistance of the pipe. For n pipes connected in parallel, the total resistance can be calculated with the formula

$$R_{tot} = \frac{1}{(\sqrt{\frac{1}{R_1}} + \sqrt{\frac{1}{R_2}} + ... + \sqrt{\frac{1}{R_n}})^2}.$$

For n pipes in serial the total resistance is the sum of the partial resistances:

$$R_{tot} = R_1 + R_2 + ... + R_n$$

4 System Modeling

With the acquired knowledge from Section 3 a mathematical model of the system can be derived.

The system is derived using the mass flow, since it is, compared to the volume flow, the more general description, because it does not depend on the density, which again, depends on the temperature. The mass flow can be calculated by multiplying the volume flow with the air density. The air density is not constant over the temperature, therefore a function representing the air density over the temperature is required. Such a function is calculated using a linear fitting from known data points, the resulting function

$$\rho(T) = -0.004395\,T + 1.23$$

is used to calculate the mass flow from the volume flow of air at a specific temperature and vice versa. The data points are shown in Figure 16.

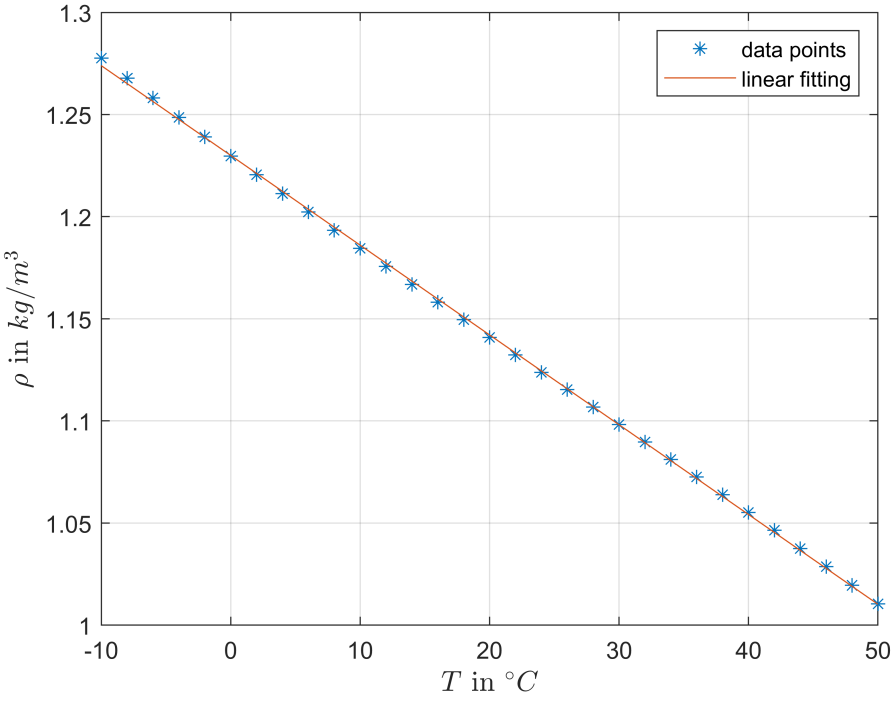

Figure 16: Air density as function of the temperature at $965mbar$ and 60% relative humidity. Data points computed with "CoolProp 6.4.1".

The values of the air density are only approximated, since the air density depends on many other factors as well. The water density does not vary much and is assumed to be constant.

Furthermore, the HVAC-box is assumed to be an adiabatic wall.

4.1 Blower Motor Modeling

The main task of the blower motor is the transportation of the air, but the heating of the motor might have an impact on the air temperature as well. Both aspects have to be analysed.

4.1.1 Blower motor Heating

To determine the impact of the blower motor on the air temperature, an experiment was made. With deactivated electric heater and chiller, the motor was put under tension. The resulting measurements are shown in Figure 17.

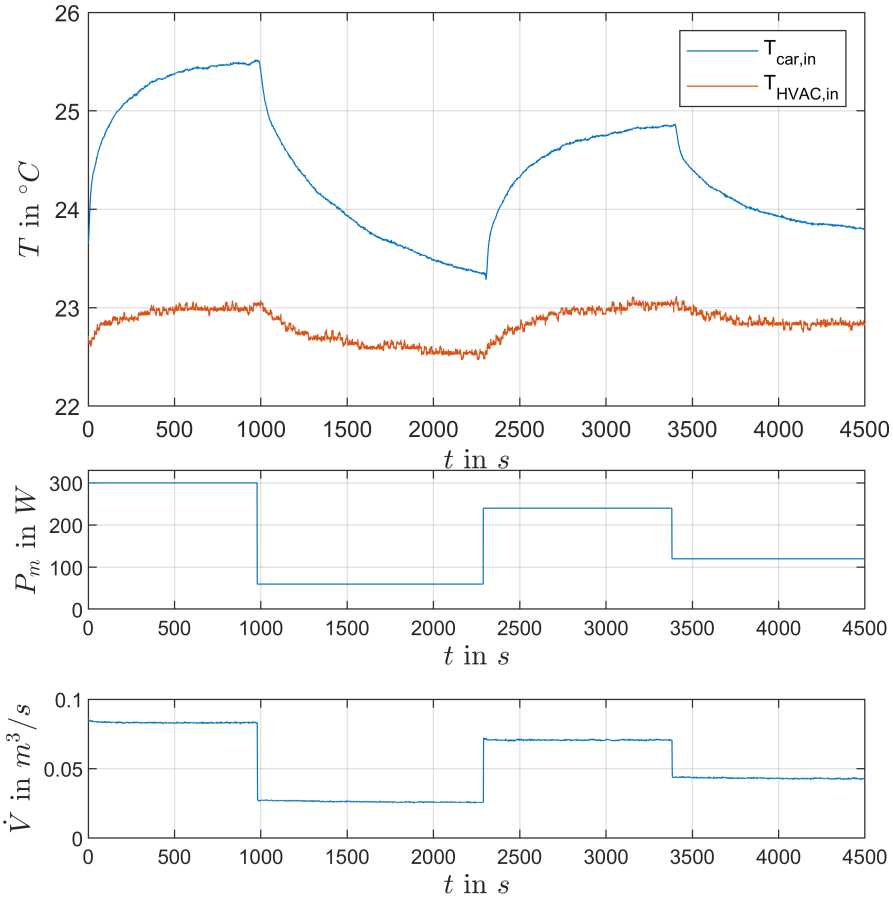

Figure 17: Blower motor measurement to determine the air heating. The electric power P_m was not measured, but is an estimated mean value.

In this experiment, a thermocouple was used to measure the temperature of the air entering the car $T_{car,in}$. The increase in the temperature of the blower motor causes an increase in the air temperature of more than $2°C$ at maximum power. This can not be neglected.

From the measurement shown in Figure 17 the data points shown in Figure 18 can be derived by computing the steady state mean of the four measurements.

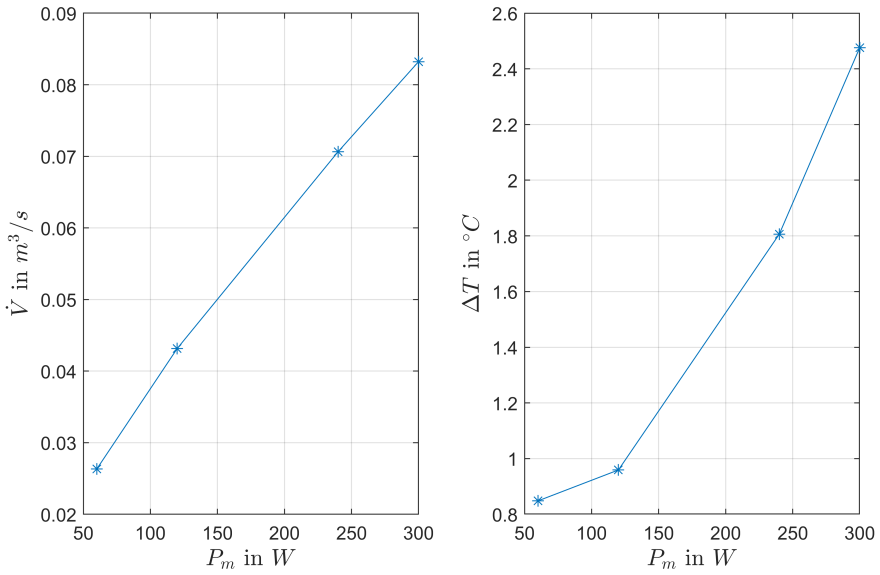

Figure 18: Volume flow on the left, change in temperature on the right, both as function of blower motor power. The values are calculated steady state values from 17.

The resulting volume flow $\dot{V}$ in respect to the input power is shown on the left. The dependency is assumed linear.

On the right, ΔT denotes the increase in temperature caused by the blower motor at the respective power. For the lowest input power, the steady state was not reached completely, so in this case the temperature difference ΔT is a bit lower than the data point measurement shown in the Figure. The dependency is not linear.

As it can be observed in Figure 17, the heating is a lot faster than the cooling of the air. The reason for that is, that the electric current heats the motor, but the only way for the motor to cool down is to transfer the heat to its surroundings, since it is not positioned in the airflow.

To describe the change of air temperature in relation to the input power, a first order lag element is used. It would be better to use two different lag elements for the heating and cooling since the dynamics are different, but since only a rough estimate is required, the time constants are assumed to be the same. The first order lag element

$$G_m(s) = \frac{K_m(P_m)}{\tau_m s + 1}$$

was used, τ_m can be described as the time constant of the blower motor heating and cooling. The gain of the transfer function K_m depends on the blower motor power and is described by the function in Figure 18 on the right.

The parameter $\tau_m s$ was identified using numerical optimization. In every iteration, the blower motor system is simulated and the error between the output of the simulation and the measurement data from 17 are calculated in the least squares sense. Starting the optimization with the value $\tau_m = 100$, an optimum is found at $\tau_m = 268$. The comparison between the simulation and the measurement is shown in Figure 19.

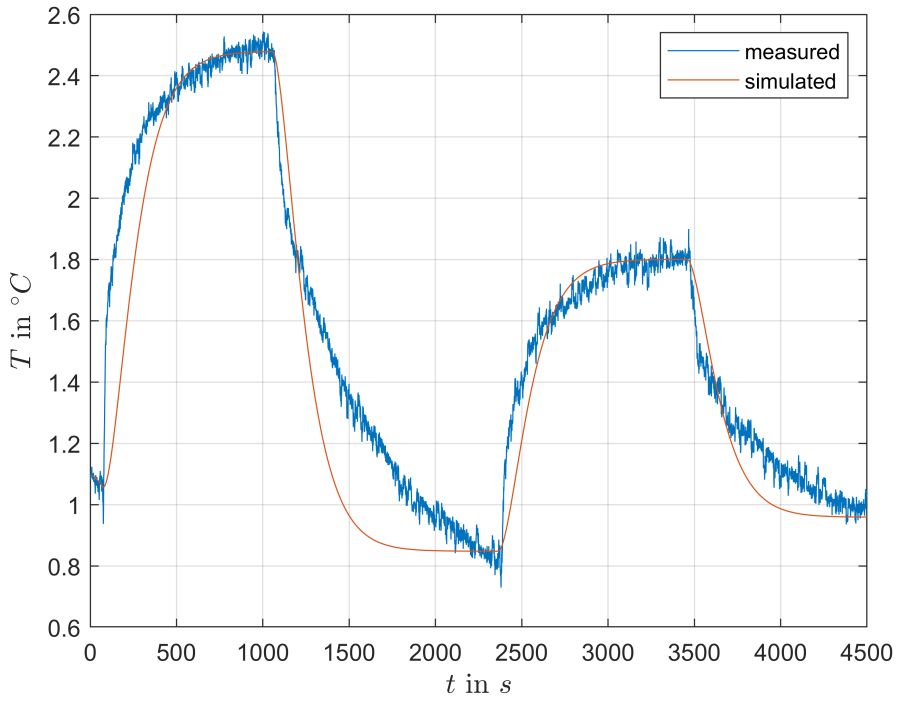

Figure 19: Comparison between simulation and measurement for the blower motor heating.

As expected, the result is not very accurate due to the assumptions made, but this rough estimate is accurate enough for the application.

4.1.2 Volume Flow

Also for the volume flow, the electric power is the input of the system. The volume flow of the blower motor can be modeled with a curve, with the electric power on the abscissa and the volume flow on the ordinate. This is a valid assumption, since the dynamics of the blower motor are very fast compared to the chosen sampling rate of one second.

A plot of the volume flow as function of the power is shown in Figure 20.

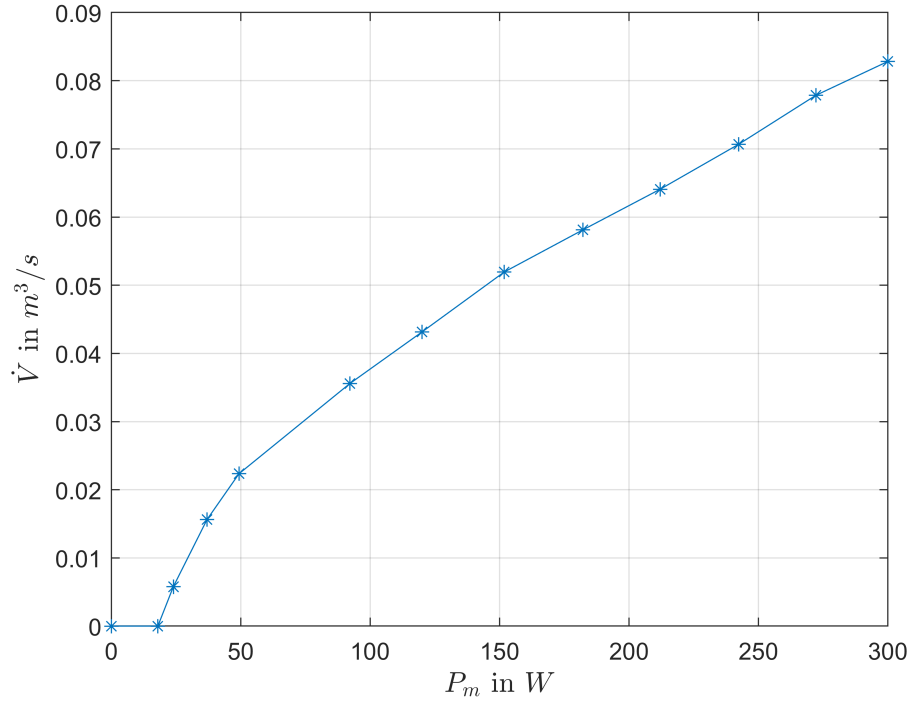

Figure 20: Volume flow generated by the blower motor as a function of the blower motor power. All valves were set on open according to Table 1.

This function is used for the plant in the simulation, with a unit delay of the sampling rate in the feedback loop.

4.2 External Water Chiller and Cooler Core Modeling

The pressure loss in the tubes and the cooler core are constant. For this reason, also the mass flow of the water has to be constant. The only input variable of the chiller is the water temperature. This temperature is controlled with a relay-controller with hysteresis. This hysteresis is neglected for the modeling. The pipes leading to the car are about $10m$ long and thermally isolated, it is therefore assumed, that the water temperature is constant until entering the cooler core.

A steady state experiment is made, to check the cooling capacity of the chiller. The result of the measurement is shown in Figure 21.

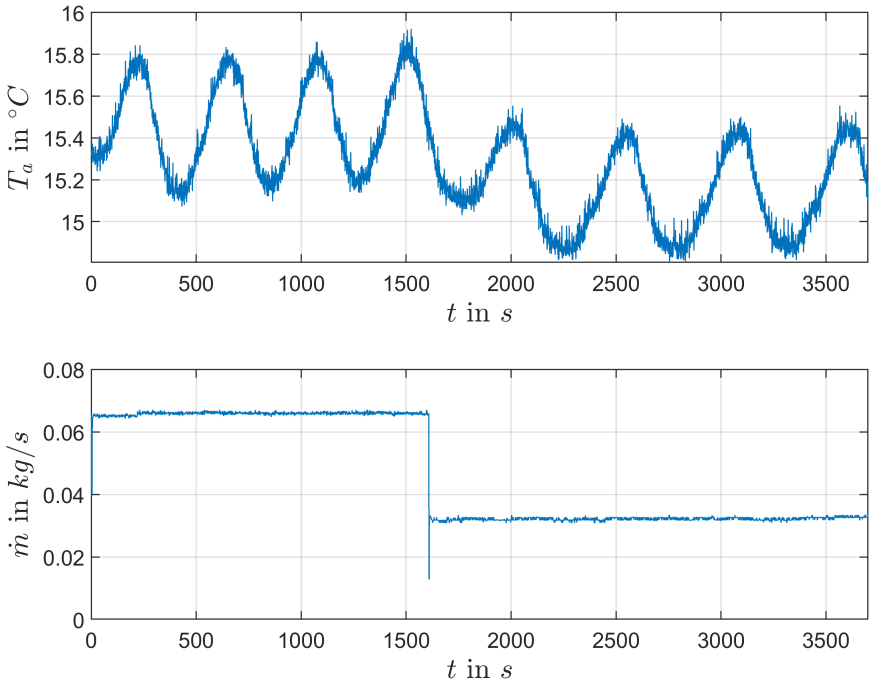

Figure 21: Impact of the mass flow on the air temperature.

The measurement illustrates that the mass flow of the air has a really low impact on the air temperature entering the car. The heat capacity of the air is too small to have an impact on the cooling capacity of the cooler core. This small deviation in the temperature is neglected. In the simulation, the temperature of the air entering the cabin only depends on the water and air temperature, but not on the mass flow.

A measurement is made to analyse the chiller dynamics. The water temperature is changed, the air temperature entering the HVAC-Box and the air temperature entering the car are measured. The result of this measurement is shown in Figure 22.

As the measurement shows, the air temperature rises and falls with a constant slope after a change in the water temperature. For this reason it can be assumed that the water temperature also changes with the same slope, which makes sense, since the chiller works with a two-point controller. A falling and a rising ramp is analysed using a linear fitting, the result is shown in Figure 23.

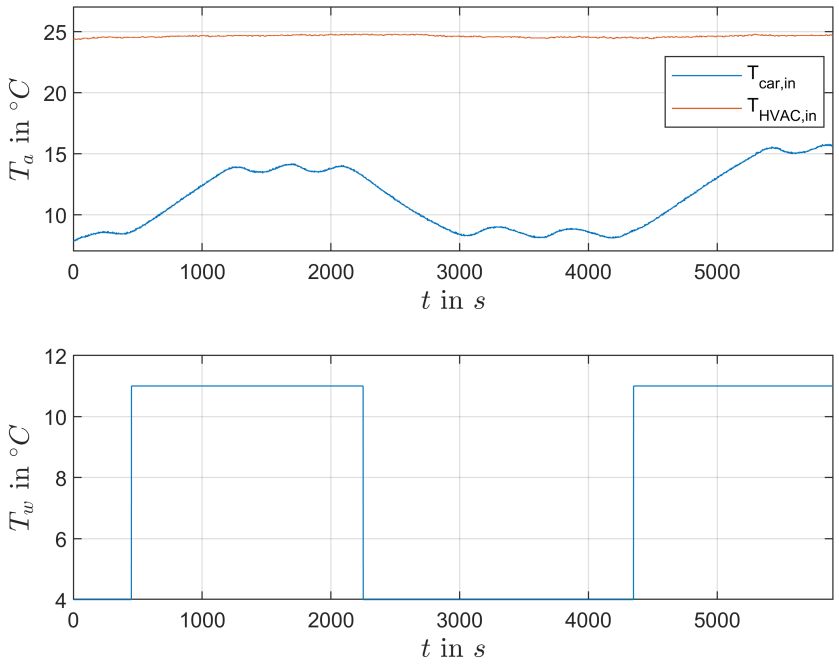

Figure 22: Air temperature measurement with changing water temperature of the chiller.

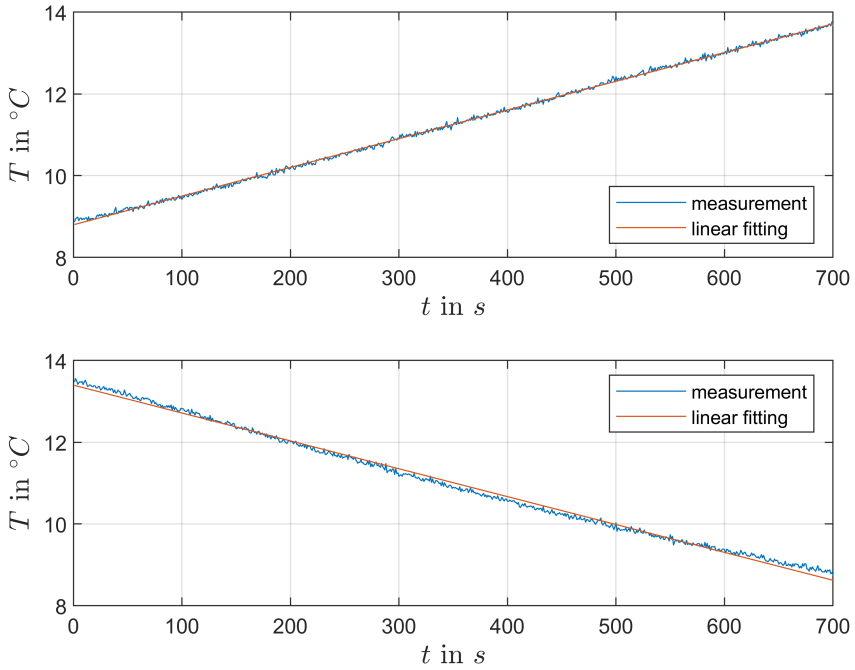

Figure 23: Chiller heating and cooling dynamics.

The rising and falling function have a slope of 0.00702 and -0.00682 respectively. The mean of absolute value of those two numbers equals 0.00692, this value is used in the model for the transition of the air temperature when a change of the water temperature occurs.

The air temperature entering the cabin takes on a value between the air temperature entering the HVAC-box and the water temperature. To determine the relationship between those two temperatures, another measurement was made. The water temperature was changed a few times, while the air temperature was measured. The measurement result is shown in Figure 24.

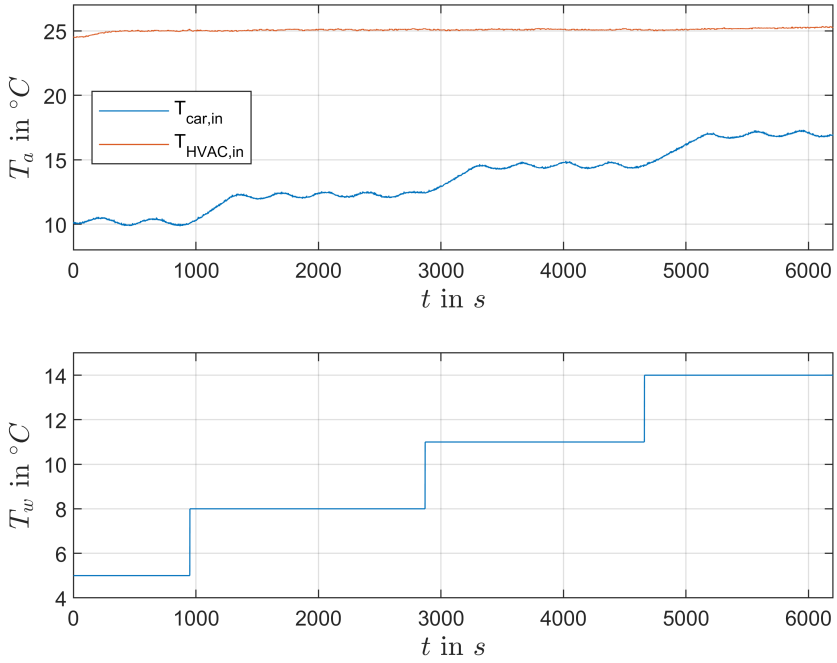

Figure 24: Air temperature for stepwise changing water temperature.

The mean value of the air temperature was calculated for every step after the air temperature settled in. The relation between the water and air temperature is shown in Figure 25.

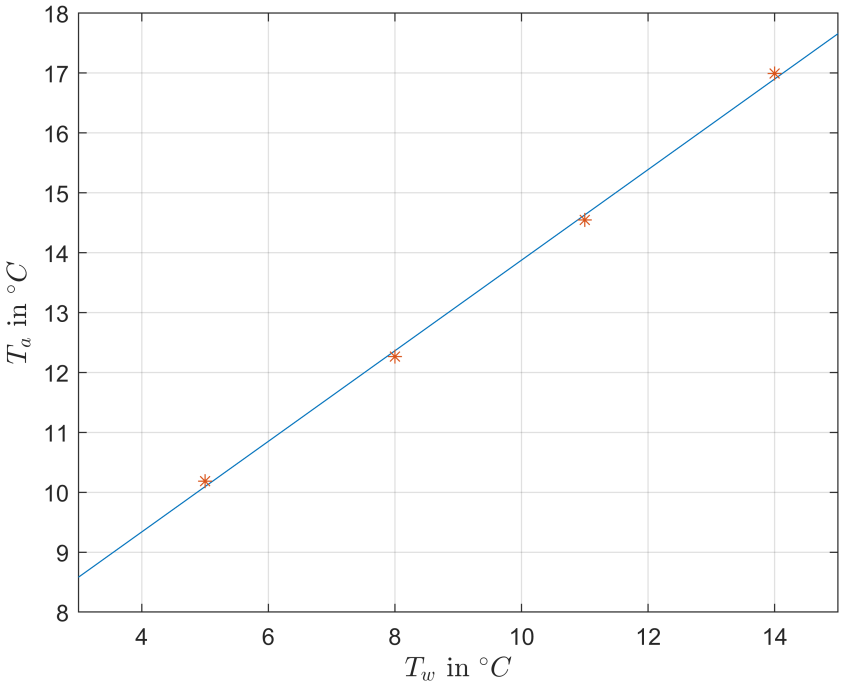

Figure 25: Air temperature as function of the water temperature.

As the measurement shows, the relation between the air temperature and the water temperature is quite linear in the steady state case. For this reason, a linear fitting was applied. The linear fitting function is

$$T_a = 0.7564 T_w + 6.312.$$

For validation purposes the experiment shown in Figure 24 was also used for simulation. The comparison between the simulation and the measurement is pictured in Figure 26.

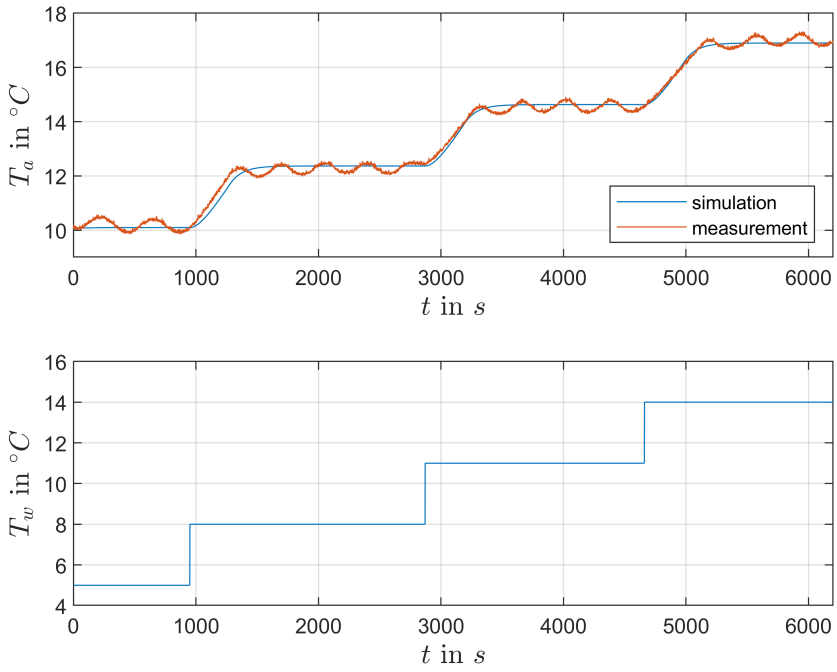

Figure 26: Comparison between simulation and measurement from the experiment shown in Figure 24

4.3 Electric Heater Modeling

Starting with the principles of energy and mass conservation from Equations (3) and (4), a physical model for the heater can be derived starting with:

$$m_a c_{p,a} \frac{dT_{a,h}}{dt} = \dot{Q}^{i,a} - \dot{Q}^{o,a},$$

with the variables m_a as the air mass in the heater, $c_{p,a}$ as the specific isobar heat capacity of the air, $T_{a,h}$ as the temperature of the air in the heater and $\dot{Q}^{i,a}$ and $\dot{Q}^{o,a}$ as the heat being added to and leaving the air.

The heat transfer $\dot{Q}^{i,a}$ can be substituted as shown by Equation (2). It is assumed that all the heat leaving the electric heater is consumed by the air mass flowing trough. The heat transfer $\dot{Q}^{o,a}$ can therefore be described as the temperature difference between the air leaving $T^o_{a,h}$ and the air entering $T^i_{a,h}$ the heater multiplied with the air mass flow $\dot{m}_a$ and the specific heat capacity of the air, i.e.,

$$m_{a,h} c_{p,a} \frac{dT_{a,h}}{dt} = k_h A_h (T_h - T_{a,h}) - c_{p,a} \dot{m}_a (T^o_{a,h} - T^i_{a,h}),$$

where k_h is the heat transfer coefficient between the heater and the air, A_h is the contact area between the heater and the air and T_h is the temperature of the heater.

Another differential equation is required to describe the dynamics of the alluminium part of the heater. The same approach as above can be used to describe the heater dynamics. Hence

$$m_h c_h \frac{dT_h}{dt} = P_{el,h} - \dot{Q}^{o,h},$$

where m_h is the mass of the heater and c_h is the specific heat capacity of the heater material. All the energy entering the heater is electric power $P_{el,h}$ and all the heat leaving the heater $\dot{Q}^{o,h}$ is transferred to the air inside the heater. The electric power is described as $P_{el,h} = U_h I_h$. The dynamics of the heater can therefore be described as

$$m_h c_h \frac{dT_h}{dt} = -k_h A_h (T_h - T_{a,h}) + k_p P_{el}.$$

Since the electric heater has a low resistance, the resistance of the cables leading the current to the heater can not be neglected. For this reason the variable k_p is introduced to describe how much power is dissipated in the heater. For a better understanding, a picture of the heater and its inputs and outputs is shown in Figure 27.

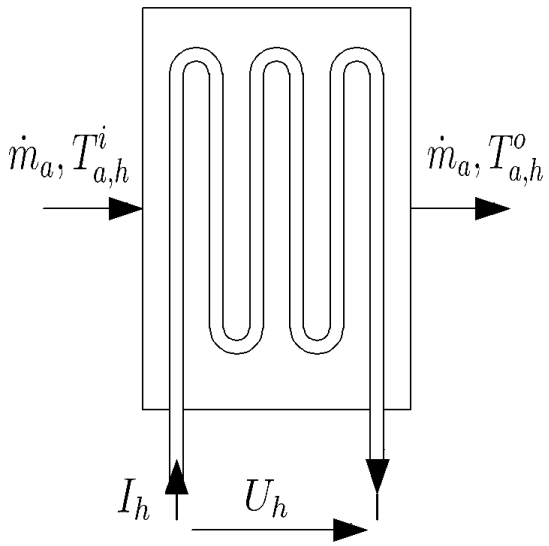

Figure 27: Modeling representation for the electric heater.

Summing up, the heater can be described as a system with three inputs, the air mass flow $\dot{m}_a$, the air temperature entering the heater $T^i_{a,h}$ and the electric power P_{el}. The two outputs of the heater are the air mass flow and the air temperature. The mass flow is assumed to be constant during the whole process, even if in reality, it changes slightly with the air temperature because of the change in the air density. This error is neglected in the presented model. The air temperature in the heater is assumed to be perfectly mixed, for this reason the air leaving the heater is assumed to have the same temperature as the air inside the heater, therefore $T^o_{a,h} = T_{a,h}$.

By combining the two parameters k_h and A_h as $k_{A,h} = k_h A_h$ and rearranging the two differential equations, the final model for the heater can be described as

$$\frac{dT_{a,h}}{dt} = \frac{k_{A,h}}{m_{a,h}c_{p,a}}(T_h - T_{a,h}) - \frac{\dot{m}_a}{m_{a,h}}(T_{a,h} - T^i_{a,h})$$
$$\frac{dT_h}{dt} = -\frac{k_{A,h}}{m_h c_h}(T_h - T_{a,h}) + \frac{k_p P_{el}}{m_h c_h},$$

with the unknown parameters $k_{A,h}$, $m_{a,h}$, $c_{p,a}$, m_h, c_h and k_p.

4.4 Electric Heater Parameter Identification

For the parameter identification, the following parameters m_h, $c_{p,a}$, c_h, $m_{a,h}$, k_p and $k_{A,h}$ have to be identified.

The identification of the mass of the electric heater is just weighting its thermal mass with a scale. The measurement results in $m_h = 243g$.

The specific isobar heat capacity of air $c_{p,a}$ and the specific heat capacity of the heater c_h are temperature dependent, but this is neglected, since the temperature difference is small. The specific heat capacities are known material properties. According to [3] the values are $c_{p,a} = 1007\frac{J}{kgK}$ at $26,85°C$ and $1bar$ and $c_h = 897\frac{J}{kgK}$ for aluminium at $25°C$ and $1bar$ pressure.

Taking a look at the equations in the steady state case:

$$0 = k_{A,h}(T_h - T_{a,h}) - \dot{m}_a c_{p,a}(T_{a,h} - T^i_{a,h})$$
$$0 = -k_{A,h}(T_h - T_{a,h}) + k_p P_{el,h}$$

The two equations can be equalized on the heat transfer between the heater and the air. The only remaining unknown constant is k_p. By solving for k_p, the resulting equation for the steady state is

$$k_p = \frac{\dot{m}_a c_{p,a}(T_{a,h} - T^i_{a,h})}{P_{el}}. \tag{5}$$

The measurement from Figure 28 was made with constant Power entering the heater and stepwise changing the mass flow:

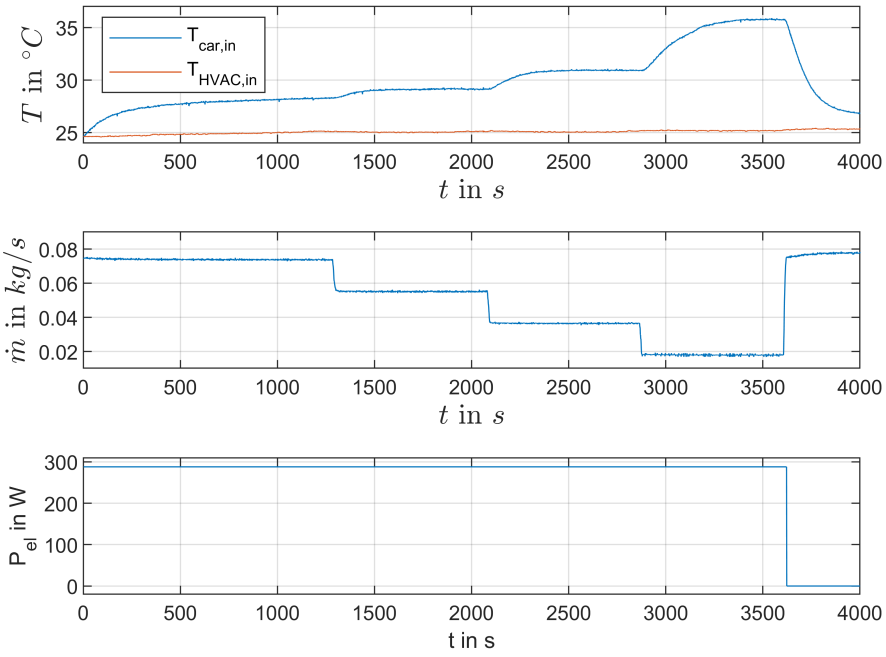

Figure 28: Steady state measurements for the electric heater.

The mean of every value was computed for the $100s$ before every step. The results are shown in Table 2.

measurement number	P_{el}	$T_{a,h}$	$T^i_{a,h}$	$\dot{m}$
	W	°C	°C	$\frac{kg}{s}$
1	288	28.3	26	0.0737
2	288	29.1	25.7	0.0551
3	288	30.9	25.4	0.0346
4	288	35.8	25.2	0.0179

Table 2: Steady state measurement results for the electric heater.

Inserting the values from Table 2 into equation 5 gives four estimates for the parameter k_p. The mean of those four estimates is $k_p = 0.669$. This value is used for the model.

The remaining two unknown parameters $m_{a,h}$ and $k_{A,h}$ were estimated using the measurement shown in Figure 29.

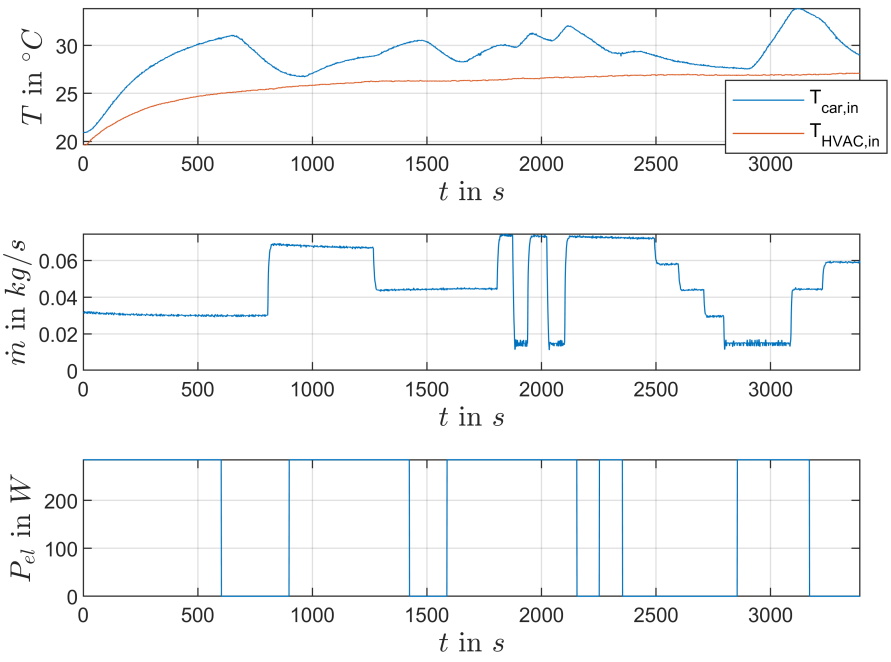

Figure 29: Measurement for the heater parameter optimization. The electric power is an estimated mean value in this case.

As shown in Figure 12, the electric power depends on the temperature of the heater. With the given setup, it is not possible to measure the electric power at all times, for this reason, the electric power is an estimated mean value and assumed to be constant.

The remaining parameters were estimated using numerical optimization, comparing the measured with the simulated air temperature in the least squares sense for every iteration. Starting the optimization with the parameters, $m_{a,h} = 20mg$, the roughly estimated volume of the air inside the heater and $k_{A,h} = 1W/K$. The optimization finds a minimum at the values $m_{a,h} = 14.21mg$ and $k_{A,h} = 2.49W/K$. The parameters are plausible.

The comparison between the result of the simulation with the estimated parameters and the measurement are shown in Figure 30.

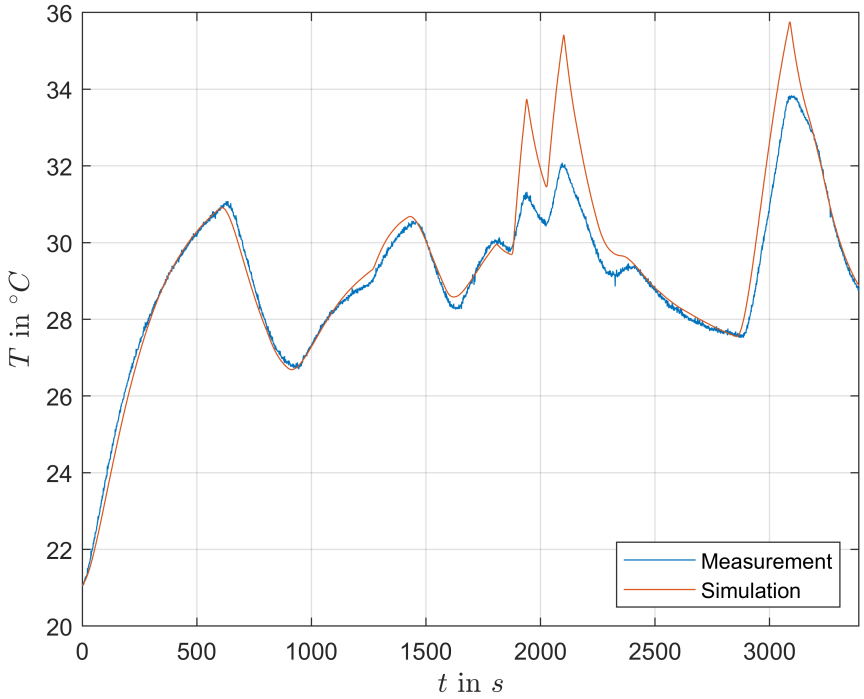

Figure 30: Simulated and measured heater outlet temperature for the measurement from Figure 29.

In general, the model seems to capture the main dynamics of the electric heater. However, the peaks drifting off are caused by the non linear behavior of the heater resistance. The low volume flow causes the temperature of the heater to rise. A higher temperature means a higher resistance of the heater, as shown in Figure 12. That means, that the heater requires less power, so in reality the current flowing trough the heater drops. In the simulation, the power is assumed to be constant, which causes the high temperature peaks.

For the purpose of validation, another measurement as shown in Figure 31 was made. The result of the comparison between simulation and measurement are shown in Figure 32.

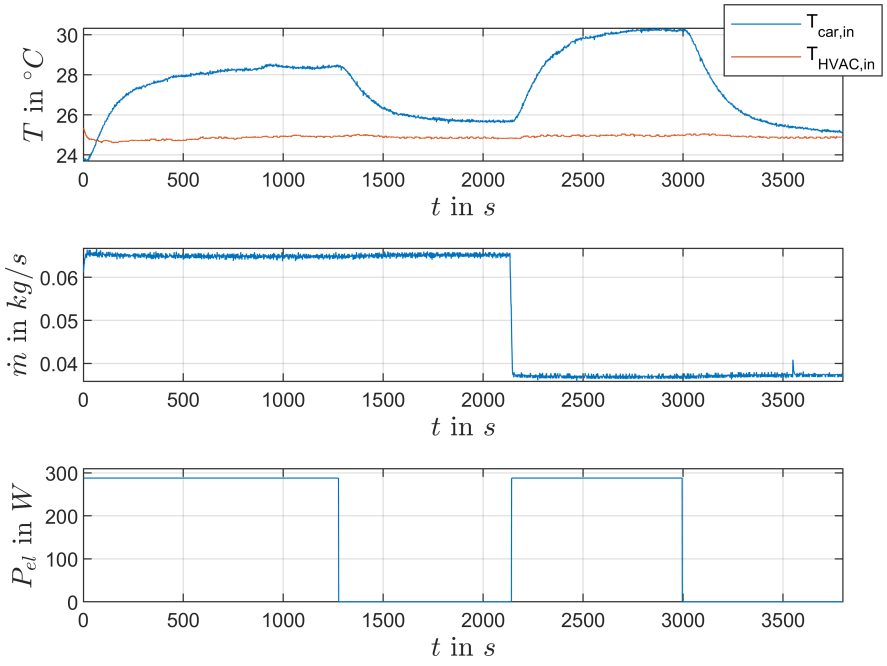

Figure 31: Validation measurement for the heater.

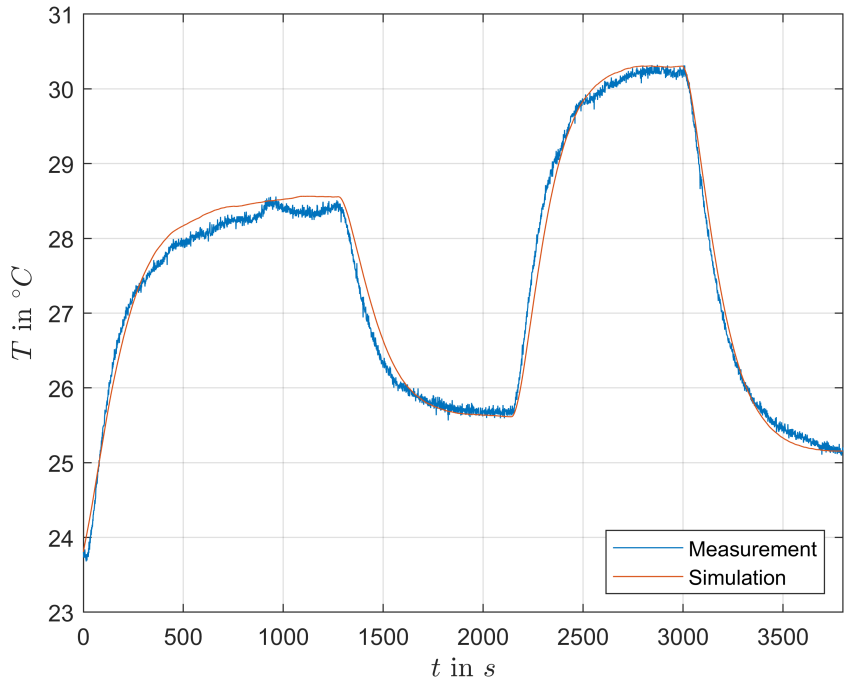

Figure 32: Simulated and measured heater outlet temperature for measurement from 31.

4.5 Valves

The three valves w, m and f have the task to distribute the air on the different car inlets. The valve a has the task to control how much air bypasses the heater and cooler core. Since the tasks are different, the valves are analysed separately.

4.5.1 Temperature Valve a

The temperature valve a is expected to have an impact on the mass flow, since the air encounters more resistance if it has to flow trough the heater and cooler core. To check how big this impact is, a measurement was made. The result is shown in Figure 33.

As the measurement shows, when the air flows trough the cooler core and the heater, the mass flow is about 10% smaller with the same input power. The volume flow controller should be able to compensate for the error.

The main task of the the valve a is to split the airflow into the two paths. To determine how much air flows trough what path, a measurement was conducted. With a constant water temperature of $5°C$ the valve position a was changed and the air temperature was measured. The measurement result is pictured in Figure 34.

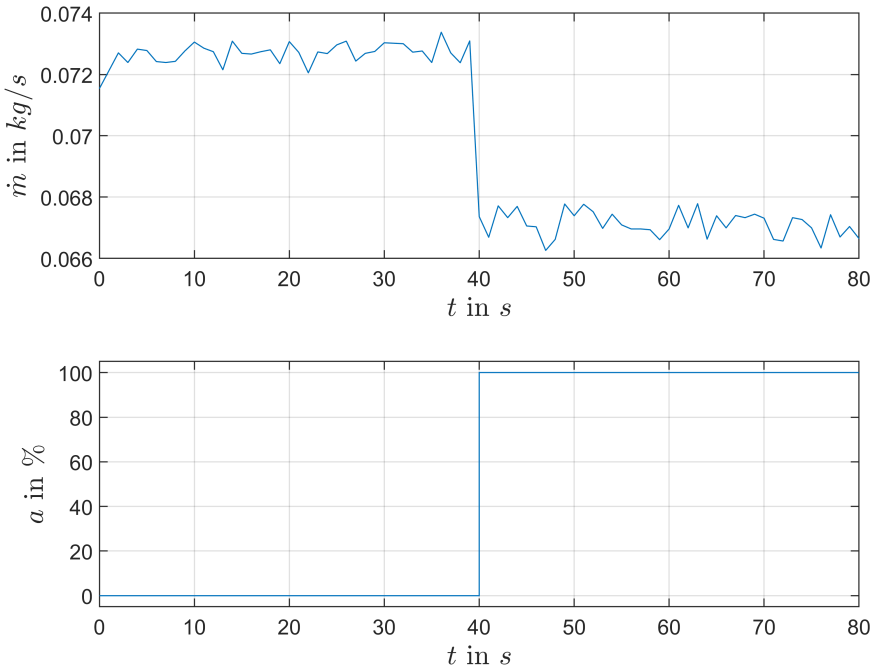

Figure 33: Impact of the temperature valve a on the mass flow.

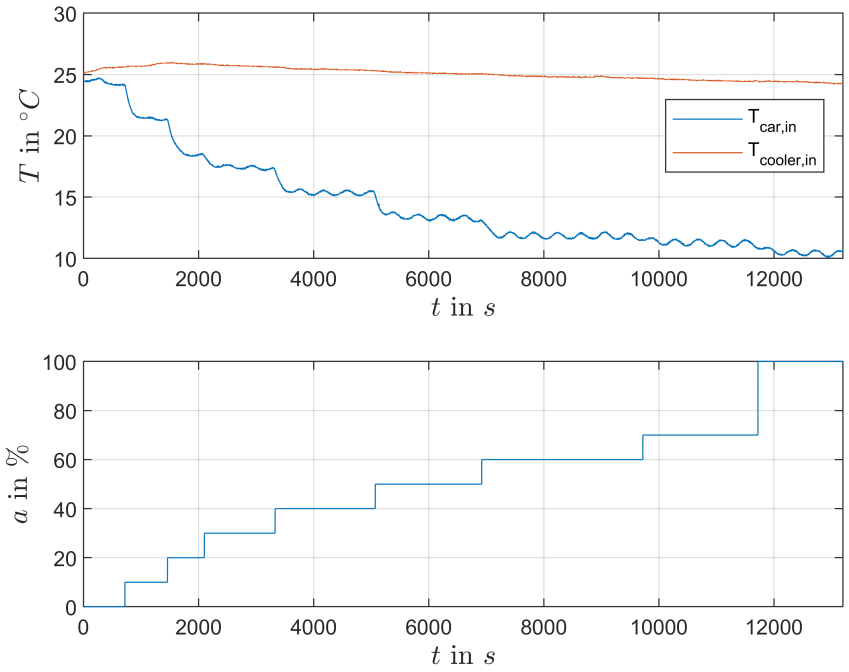

Figure 34: Measurement to estimate the impact of the temperature valve a on the air distribution.

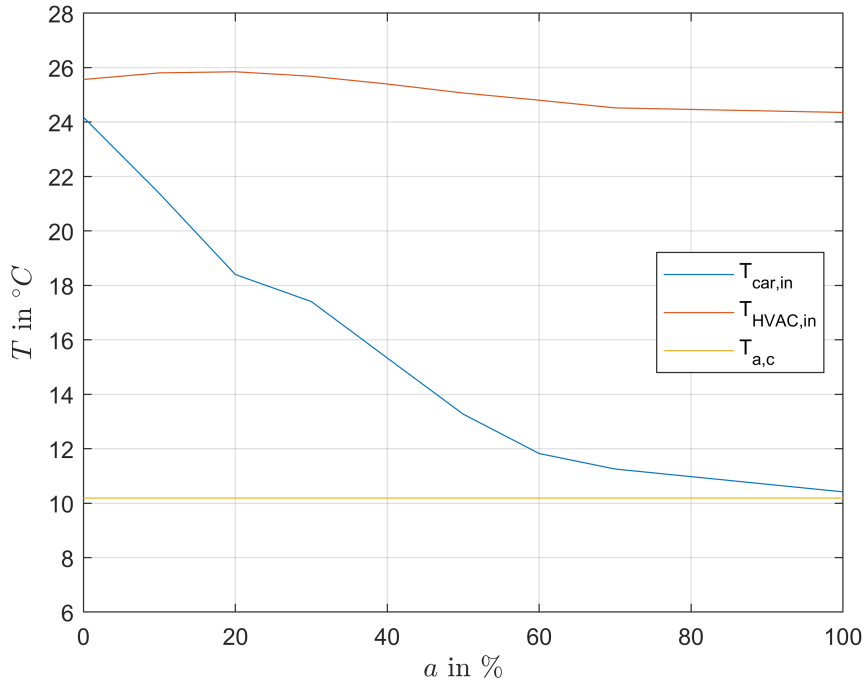

Figure 35: Temperature of the air entering the HVAC-box $T_{HVAC,in}$, temperature of the air entering the car $T_{car,in}$ and the air temperature if all the air would flow trough the cooler core $T_{a,c}$ from Figure 25 at $T_w = 5°C$.

It is to note, that the air distribution depends on the total mass flow as well. For the purpose of modeling, it is assumed that air distribution is the same for every mass flow. The mean of the air temperature was calculated for every steady state position. The result of the measurement is shown in Figure 35.

From the resulting temperature, the air distribution can be estimated for the different angles. A variable to describe the amount of air bypassing the electric heater and the cooler core in percent is introduced. This variable b can be calculated for every measured angle with

$$b = \frac{T_{car,in} - T_{a,c}}{T_{HVAC,in} - T_{a,c}}.$$

The resulting distribution is shown in Figure 36.

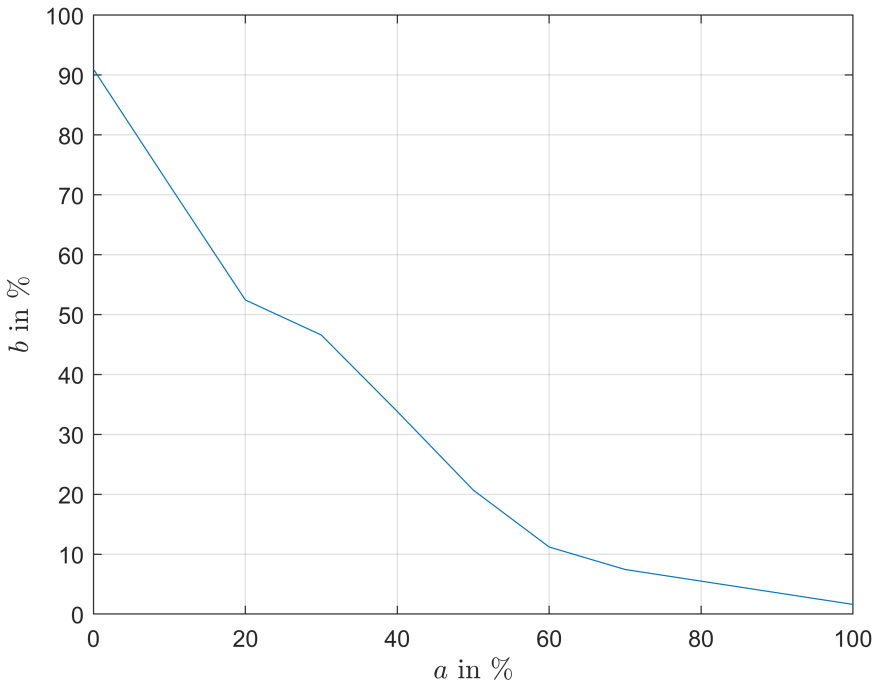

Figure 36: Air distribution b caused by the valve a.

As the measurements show, the valve does not seal perfectly, about at least 10% of the air always flows trough the cooler core and the heater. The valve does seal decently on the other side.

After splitting the air into the two paths, one of the two paths heats or cools the air, the other one does not change the air temperature. The two different mass flows $\dot{m}_1$ and $\dot{m}_2$ with the temperatures T_1 and T_2 are reunited afterwards. The resulting mass flow $\dot{m}$ equals the mass flow before the air splits into the two branches since no air loss is assumed and the change in mass flow due to the heating and cooling is neglected.

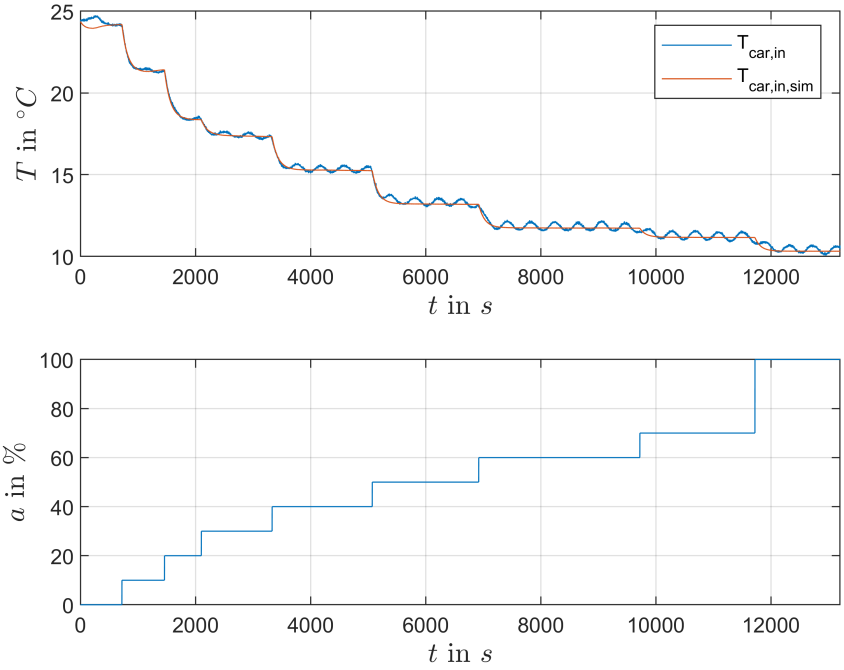

Figure 37: Comparison between measurement and simulation for experiment shown in Figure 33.

The resulting air temperature entering the car T_a can be calculated by

$$T_a = \frac{T_1 \dot{m}_1 + T_2 \dot{m}_2}{\dot{m}}.$$

A simulation with the measurement from Figure 33 was made to check the results.

4.5.2 Airflow Valves m, w, f

The other three valves on the other hand only have an impact on the mass flow at the outlets, but no effect on the temperature inside the HVAC-Box. They can, just like the valve a, increase the flow resistance. The valve control needs to be made in a way, that the valves are always as far open as possible, such that the impact on the volume flow is low. Furthermore, a lower pressure loss is easier to overcome for the blower motor and therefore requires less energy.

The airflow at the output needs to be calculated depending on the three servo motor angles f, m and w. The valves are modeled as variable resistors depending on the valve angle. The resulting system is shown in Figure 38.

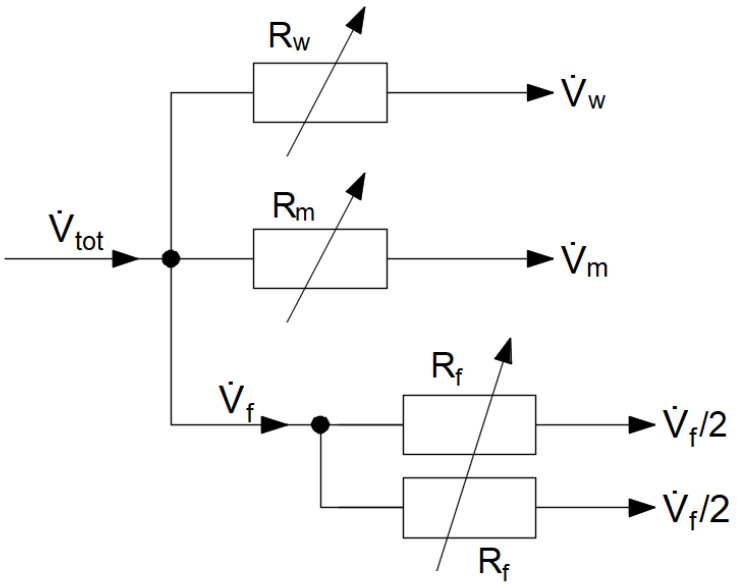

Figure 38: Flow resistances of the HVAC-Box valves.

The total volume flow is divided into four paths by the windshield valve R_w, the valve for the chest outlets R_m and the two valves for the feet outlets R_f, that can only be controlled together and therefore always have the same value. The windshield branch splits into the two defrost outlets at the side windows and the two windshield outlets in the middle. The middle branch splits into two side window outlets and two middle outlets.

Since no volume flow sensors are mounted at the outlets, a feedback control cannot be applied. Therefore a feedforward control is used estimating the resulting mass flow at the outlets. To do so, the flow resistance of the valves, as described in Section 3.2, are required for every angle.

For this purpose, a few measurements were made. With always just one valve open, and the other two completely closed, the volume flow and the pressure loss was measured, based on the angle of the valve. The resulting measurements for the valves are shown in Table 3, 4 and 5.

measurement number	m	$\dot{V}$	Δp	R_m
	%	$\frac{m^3}{s}$	Pa	$\frac{kg}{m^7}$
1	0	0.02833	186	231696
2	10	0.02861	186	227218
3	20	0.02861	184	224775
4	30	0.02889	182	218077
5	40	0.02972	172	194700
6	50	0.03833	236	160605
7	60	0.04194	182	103448
8	70	0.04583	137	65217
9	80	0.04944	87	35586
10	90	0.05111	59	22585
11	100	0.05167	44	16483

Table 3: Measurements to determine the valve resistance R_m.

measurement number	f	$\dot{V}$	Δp	R_f
	%	$\frac{m^3}{s}$	Pa	$\frac{kg}{m^7}$
1	0	0.02778	178	230688
2	3	0.02778	179	231984
3	6	0.02806	176	223602
4	9	0.02833	177	220484
5	12	0.02833	176	219239
6	15	0.02889	167	200104
7	18	0.03667	232	172562
8	21	0.03778	220	154152
9	24	0.04000	190	118750
10	27	0.04444	133	67331
11	30	0.04472	113	56498
12	40	0.04528	83	40486
13	50	0.04833	57	24400
14	60	0.05000	37	14800
15	70	0.05000	38	15200
16	80	0.05056	36	14085
17	90	0.05056	35	13694
18	100	0.05139	30	11360

Table 4: Measurements to determine the valve resistance R_f.

measurement number	w	$\dot{V}$	Δp	R_w
	$\%$	$\frac{m^3}{s}$	Pa	$\frac{kg}{m^7}$
1	0	0.02833	173	215502
2	10	0.02833	170	211765
3	14	0.02833	170	211765
4	18	0.02889	170	203698
5	22	0.03861	217	145558
6	26	0.04083	181	108555
7	30	0.04306	159	85771
8	40	0.04667	122	56020
9	50	0.04917	77	31853
10	60	0.05056	52	20345
11	70	0.05139	40	15147
12	80	0.05167	35	13111
13	90	0.05194	30	11118
14	100	0.05194	31	11489

Table 5: Measurements to determine the valve resistance R_w.

For a better overview, the three calculated valve resistances as function of the angle are shown in Figure 39.

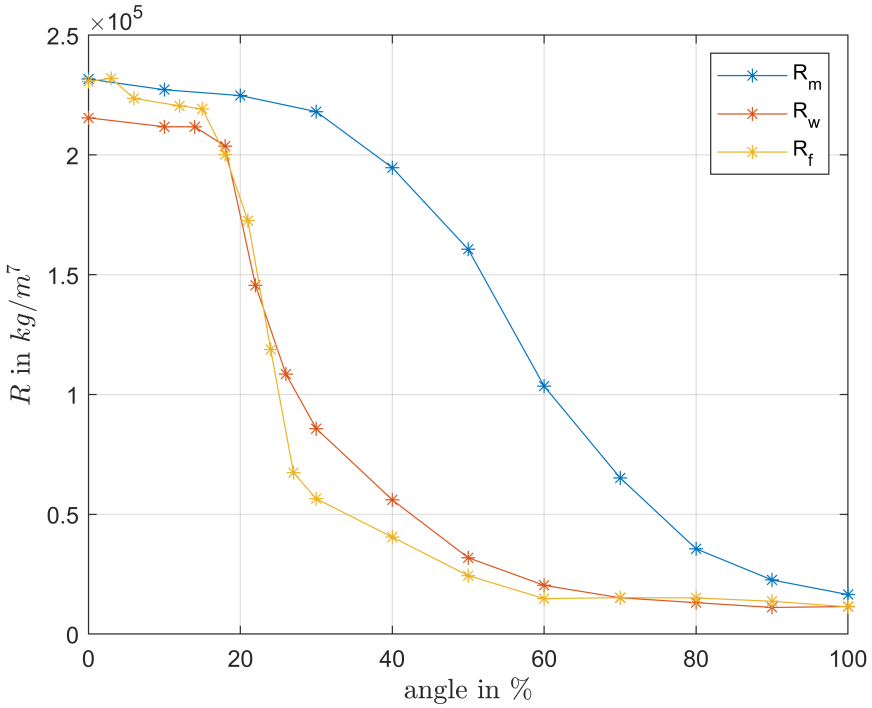

Figure 39: Valve resistance measurement results.

As the curves show, the valves for the windshield and the feet have similar curves with a steeper angle. To increase the accuracy, more measurements were made in the steeper region. The curve for the middle console is not that steep, therefore measuring in 10% steps was enough.

5 Control

A controller for the different tasks is designed in this section. A feedback control for the total volume flow and for the temperature and a feedforward control for the air distribution on the different outlets.

5.1 Total Volume Flow

The measured volume flow is fed back to compute the error to the desired volume flow. The analog input voltage for the power controller is used as input. A discrete time PI-controller with the input

$$u_v(k+1) = k_{p,v}e(k) + k_{i,v}\sum_{i=1}^{k} e(i)$$

is used. Based on the simulation, the two parameters for the controller were chosen as

$$k_{p,v} = 0.006\frac{Vs}{m^3} \qquad \text{and} \qquad k_{i,v} = 0.005\frac{Vs}{m^3}.$$

No anti-windup was used for the controller since the reference signal given by the adaptive comfort control is bounded by the possible upper and lower values, furthermore the blower motor is fast enough to never be in the saturation for a longer period of time. The comparison between the simulation and the measured values for a given reference signal is shown in Figure 40.

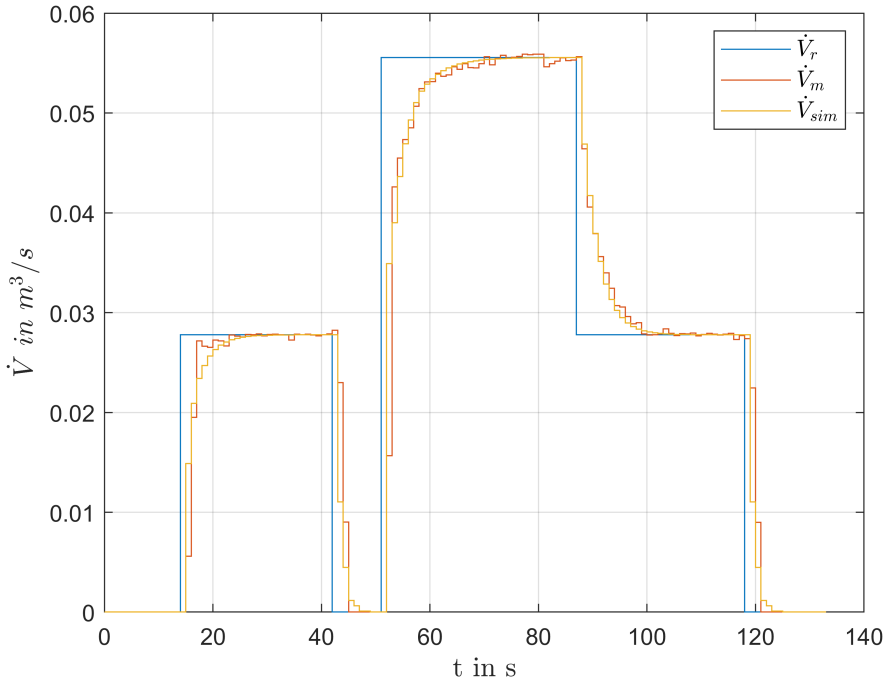

Figure 40: Comparison between the measured volume flow $\dot{V}_m$ and the simulated volume flow $\dot{V}_{sim}$ for a given reference $\dot{V}_r$.

A better control could be reached with a higher sampling rate, but the result is easily satisfactory for the given purpose.

5.2 Outlet Volume Flow

The task is to reach a requested volume flow for every outlet of the HVAC-Box. It is difficult to find an analytic solution for this problem, since there are constraints on the possible volume flows given by the flow resistances of the valves and the reference might not always be achievable. For this reason, the problem is formulated as optimization problem with the cost function

$$J(R_m, R_f, R_w) = \left(\dot{V}_m(R_m, R_f, R_w) - \dot{V}_{m,r}\right)^2 + \left(\dot{V}_f(R_m, R_f, R_w) - \dot{V}_{f,r}\right)^2 + \left(\dot{V}_w(R_m, R_f, R_w) - \dot{V}_{w,r}\right)^2 + \gamma \Delta p$$

and the three optimization variables R_m, R_f and R_w. The variables $\dot{V}_{m,r}$, $\dot{V}_{f,r}$ and $\dot{V}_{w,r}$ are the reference values for the corresponding volume flows respectively.

The pressure loss Δp and it's weighting factor γ was added to the cost function for energy efficiency, meaning that the lowest pressure loss is desired, such that the blower motor does not need to overcome unnecessary resistances to reach the desired total volume flow $\dot{V}_m$. The value $\gamma = 10^{-7}$ was chosen empirically.

The Volume flows $\dot{V}_m$, $\dot{V}_f$ and $\dot{V}_w$ can be calculated using the resistance values and the total volume flow $\dot{V}_{tot}$. According to Section 3.2, the total resistance can be calculated with

$$R_{tot} = \frac{R_m R_f R_w}{(\sqrt{R_m R_f} + \sqrt{R_m R_w} + \sqrt{R_w R_f})^2}.$$

With the measured total volume flow, the pressure loss can be calculated as

$$\Delta p = R_{tot} \dot{V}_{tot}^2.$$

Finally, the volume flows at the single outlets can be calculated with

$$\dot{V}_m = \sqrt{\frac{\Delta p}{R_m}}, \qquad \dot{V}_f = \sqrt{\frac{\Delta p}{R_f}} \qquad \text{and} \qquad \dot{V}_w = \sqrt{\frac{\Delta p}{R_w}}.$$

The lower bound

$$R_{lb} = [44600 \quad 56500 \quad 35600]$$

and upper bound

$$R_{ub} = [231000 \quad 234500 \quad 247000]$$

for the resistances were chosen based on the results shown in Figure 39. The starting value was chosen to be the same as the lower bound. This optimization problem has to be solved for every time step. When the resistances are known, the angles m, f and w can be calculated using the results from Figure 39.

5.3 Outlet Volume Flow Validation

To check the quality of the solution for the volume flow at the outlets with a specific valve angle, a few measurements are made. To do so, the velocity of the air at all the outlets is measured for every specific setup. With the knowledge of the area of the outlets, the volume flow can then be estimated.

The velocity of the air at the outlets is not constant over the whole area, therefore the velocity of the air was measured at more points of every outlet and the mean was computed. The angles were chosen such, that the resistance equals 1/3 and 2/3 of the resistance between the maximum and minimum resistance value for each valve. The result of the measurements is shown in table 6.

Nr.	α	β	γ	$\dot{V}$	v_{mm}	v_{mf}	v_f	v_{wd}	v_{ww}
	%	%	%	$\frac{m^3}{s}$	$\frac{m}{s}$	$\frac{m}{s}$	$\frac{m}{s}$	$\frac{m}{s}$	$\frac{m}{s}$
1	100	0	0	0.0547	3.03	5.78	1.03	0.18	0.40
2	100	100	0	0.0572	2.21	4.24	3.58	0.04	0.31
3	0	100	0	0.0539	0.97	1.16	6.58	0.14	0.36
4	0	100	100	0.0569	0.64	0.56	3.56	2.08	4.71
5	0	0	100	0.0542	0.82	0.88	1.16	2.37	6.03
6	50.11	21.84	21.87	0.0433	1.29	2.91	2.10	0.53	1.68
7	63.98	26	32.11	0.0517	1.48	4.00	1.58	2.71	1.28
8	51.11	21.84	100	0.0556	0.75	1.89	1.30	6.18	2.47
9	100	21.84	21.87	0.0558	3.19	5.43	1.41	0.42	1.33
10	50.11	100	21.87	0.0553	0.98	1.94	5.42	0.38	1.26
11	63.98	21.84	0	0.0464	1.64	4.40	2.13	0.15	0.38
12	0	26	21.87	0.0328	1.31	1.49	2.22	0.40	1.93
13	50.11	0	32.11	0.0389	0.95	2.17	1.40	1.13	2.49

Table 6: Outlet air velocity measurement.

The variables v_{mm}, v_{mf}, v_f, v_{wd} and v_{ww} are the mean air velocity at the middle panel outlet, the window outlet, the feet outlet, the defrost outlet and the windshield outlet respectively.

The area of the outlets can be measured, but that has shown to be rather difficult because of the form and geometry of the outlets. The measured areas of the outlets A_m formulated as vector with A_{mm}, A_{mf}, A_f, A_{wd} and A_{ww} as the single outlets from top to bottom are

$$A_m = [32.81 \quad 32.81 \quad 34.59 \quad 8 \quad 25.9]^T cm^2.$$

The outlet areas can also be calculated using the measurements from Table 6 and the matrix notation

$$SA_c = \dot{V}, \qquad \text{with} \qquad S = \begin{bmatrix} v_{mm} & v_{mf} & v_f & v_{wd} & v_{ww} \end{bmatrix}$$

where A_c is a vector with the areas of the outlets. Since perfect symmetry is assumed, only half the total volume flow is used for the calculations. The overdetermined linear system can be solved by computing the Moore–Penrose inverse of the matrix S. The resulting calculated areas of the outlets are

$$A_c = [12.13 \quad 30.6 \quad 31.31 \quad 17.55 \quad 23.88]^T cm^2.$$

With the two vectors A_m and A_c, the volume flow escaping the three valves can be calculated. These values are to be compared to the volume flow calculated using the resistances from Figure 39 for the different valve angles. The results for the volume flow with the measured area $\dot{V}_m$, the volume flow with the calculated area $\dot{V}_c$ and the volume flow calculated using the resistances $\dot{V}_R$ are shown in Figure 41.

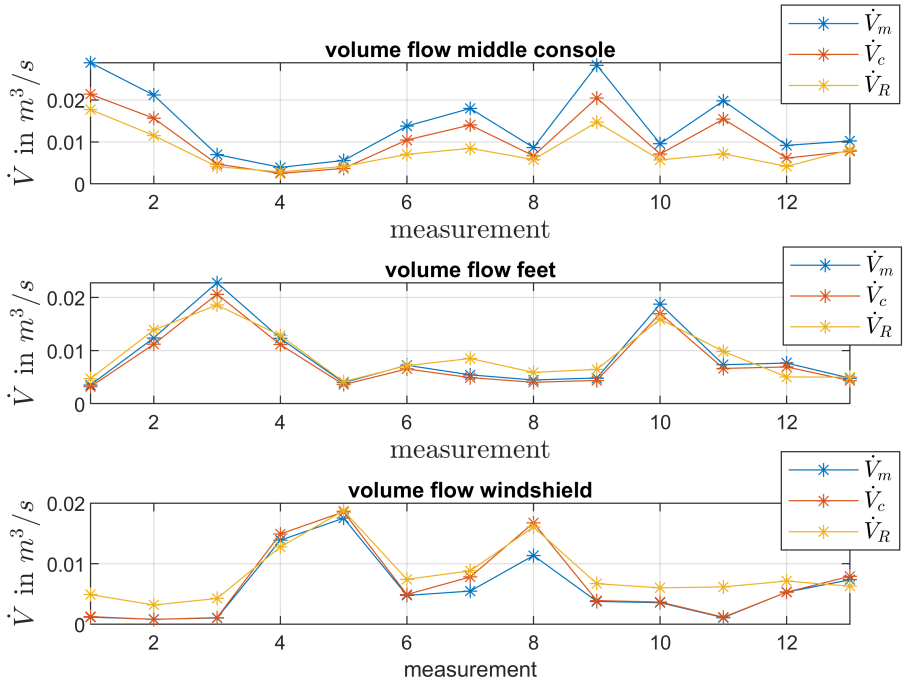

Figure 41: Volume flow at the different outlets for the different measurements.

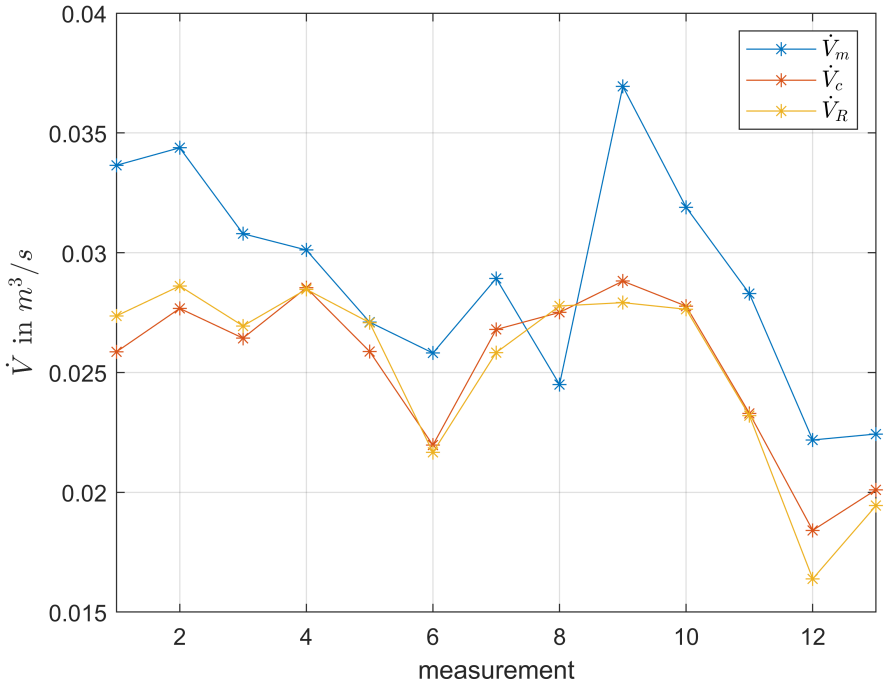

Figure 42: Total volume flow for the different measurements.

The value for $\dot{V}_m$ is larger for the middle valve and smaller for the windshield valve. To further analyse the problem, the total volume flows are calculated. The total volume flow is a measured quantity and can therefore give a reasonable reference. The result is shown in Figure 42.

The calculation of $\dot{V}_R$ is based on real measurements only, hence the computed value is reliably close to the real value. The volume flow using the calculated value $\dot{V}_c$ is close to the real value. The volume flow using the measured areas $\dot{V}_m$ on the other hand is larger for most of the measurements.

There are a few possible causes for this error. First, the areas of the outlets are hard to measure due to their geometry. Second, the air velocity measurements are uncertain for low air velocities, since the anemometer used has an absolute uncertainty. The last and most reasonable cause is the flow profile. The air velocity was always measured in the middle of the outlet grid, where for every flow profile, the airflow is always the largest. For this reason, the measured volume flow is larger for most of the values.

5.4 Temperature

The electric heater and the cooler core are in the same path. If the temperature needs to rise, the heater needs to be activated and the air needs to flow trough the heater. If the evaporator core is active on the other hand, the air needs to bypass the cooler core to rise its temperature. For the valve a to know in which direction to move, two control modes are required, a cooling mode and a heating mode.

5.4.1 Cooling mode

The only input to control the temperature in the cooling mode is the position of the valve a, since the temperature of the chiller is not changed.

With the evaporator core model from Section 4.2, a PI-controller with anti-windup was designed:

$$u(k+1) = k_{p,v}e(k) + \sum_{i=1}^{k} k_{i,v}e(i) + k_{aw}(u(i) - u_{sat}(i))$$

The input u is limited by the lower bound 0% and the upper bound 100%, which represent the limitation of the temperature valve. After several simulation trials, the parameters

$$k_p = 3\frac{\%}{^\circ C}, \qquad k_i = 0.09\frac{\%}{^\circ C} \qquad \text{and} \qquad k_{aw} = 0.1$$

were chosen. The comparison between measurement and simulation is shown in Figure 43.

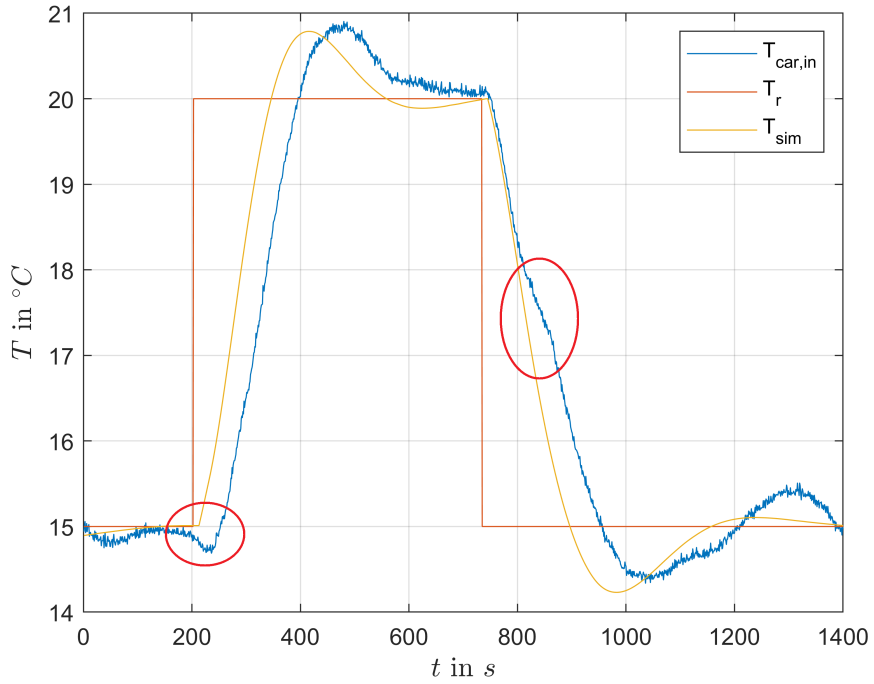

Figure 43: Comparison between the air temperature of the measured and simulated control loop. The errors caused by the chiller are marked with red circles.

The delays in the measurement are caused by the hysteresis of the chiller. As the first step occurs, the chiller turned on, so the water temperature began to lower, it took the controller a while to compensate for the falling water temperature resulting in the delay of the first step. On the second step, the chiller turned off, so the temperature began to rise. The chiller does have an impact on the step response if the timing is unfortunate, but the control can easily compensate for the hysteresis in the steady state case.

The control is too slow for the purpose. The actuator is really fast for the chosen sampling rate. The heat capacity of the air inside the HVAC-Box is quite small, compared to the cooling capacity of the cooler core. Summing up, the only reason for the control to be that slow, is that the sensor dynamics are so slow. A faster control should be possible using a faster sensor. For this reason, the sensor inside the HVAC-Box is replaced with a thermocouple.

To avoid oscillations in the temperature measurement, a drop of glue was placed on the thermocouple to raise its heat capacity and reduce the oscillation. An alternative solution would be filtering the signal, which would give the possibility to pick the time constant, but since temporal accuracy is not required, the glue method was chosen for being faster. To find the dynamics of the thermocouple and the air mixing, the same experiment as in Section 2.4 is made. Again, the time constant of the thermocouple is determined using numerical simulation. The comparison between measurement and simulation is shown in Figure 44.

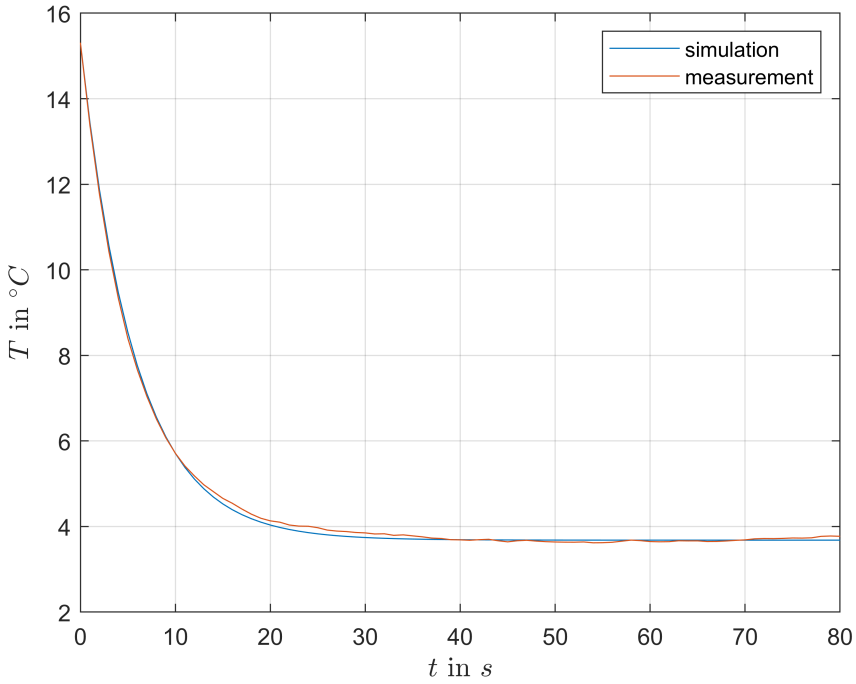

Figure 44: Comparison between the measured and simulated air temperature for the thermocouple.

The resulting time constant of the thermocouple equals $\tau_{TC} = 5.73s$. The time constant is about 17 times smaller than the one of the previous sensor.

A new controller was designed using the thermocouple results. To reduce the oscillations of the sensor, a PID-controller was used this time around. After several trials, the parameters

$$k_p = 7\frac{\%}{^\circ C} \qquad k_i = 1\frac{\%}{^\circ C} \qquad k_d = 2\frac{\%}{^\circ C} \qquad k_{aw} = 1$$

were chosen. Again, the comparison between measurement and simulation is shown in Figure 45.

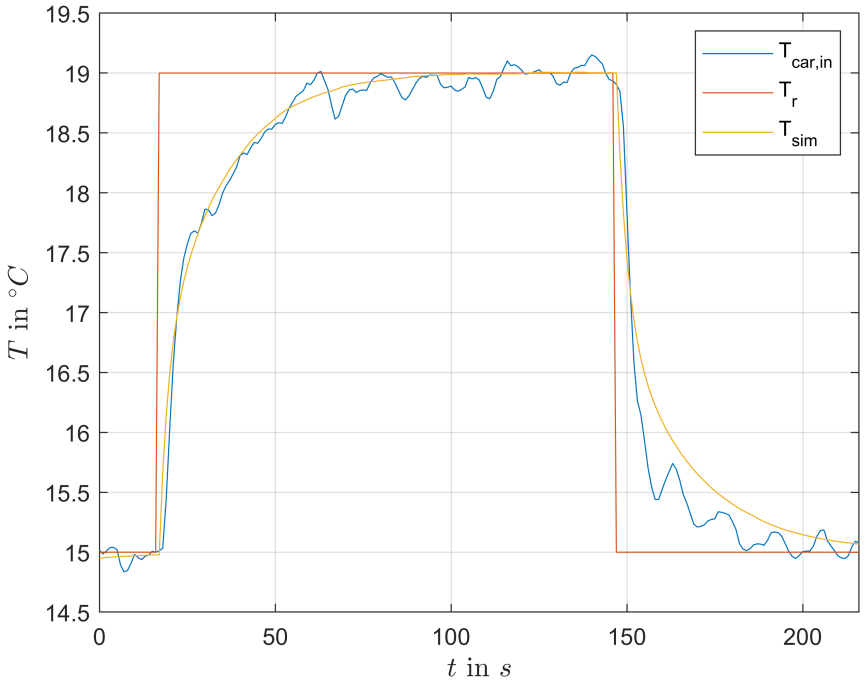

Figure 45: Comparison between the air temperature of the measured and simulated control loop using the thermocouple.

Compared to the slow sensor, the rise time of the temperature was reduced from about $400s$ to about $60s$. This control satisfies the required conditions for this project.

5.4.2 Heating mode

For the heater on the other hand, there are two inputs, the angle of the valve a and the power dissipated by the heater. The power is controlled using a power controller with a $0-5V$ analogue input signal. A PI-controller is used for the heater and a PID-controller for the temperature valve a.

Again using the model for the electric heater from section 4.3 the parameters for the two controller were chosen. For the real application, the parameters were adapted and chosen as follows:

For the valve a the parameters were chosen as

$$k_p = 7\frac{\%}{°C} \qquad k_i = 0.5\frac{\%}{°C} \qquad k_{aw} = 1.$$

For the electric heater on the other hand, the parameters were chosen as

$$k_{p,h} = 1.5\frac{V}{°C} \qquad k_{i,h} = 0.05\frac{V}{°C} \qquad k_{aw} = 0.5.$$

A measurement of step response of the result is shown in Figure 46. The simulated

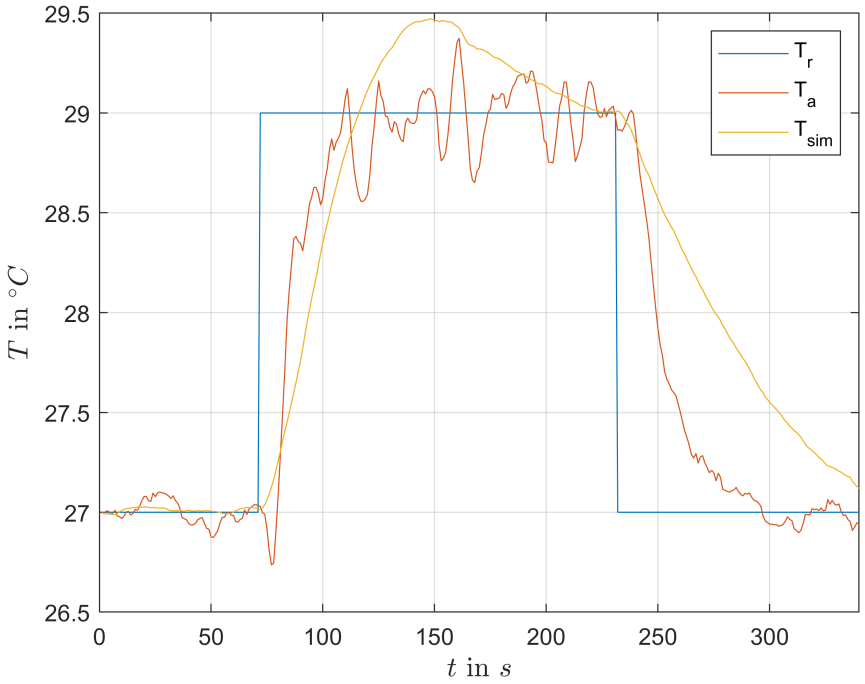

Figure 46: Comparison between the measured and simulated air temperature in the heating mode control.

result is slower than the real application. It is assumed that the real air mass inside the heater is smaller than the estimated one, that makes the dynamics faster.

Since the heater has a small heating capacity, it can easily happen, that the temperature valve a sends all the air trough the heater for a longer period of time. When this happens, some air gets trapped by the temperature valve due to its geometry. This air is heated by the heater. When the valve leaves the position the hot air is released. This causes a large error in the temperature. A measurement of such a case is shown in Figure 47. To suppress this error, the temperature valve was limited to a maximum of 80% in heating mode.

This error does not occur in the cooling mode control, because the cooling capacity is a lot higher and the desired temperature is therefore reached a lot faster. For this reason, the temperature valve does not remain in saturation for a longer period of time.

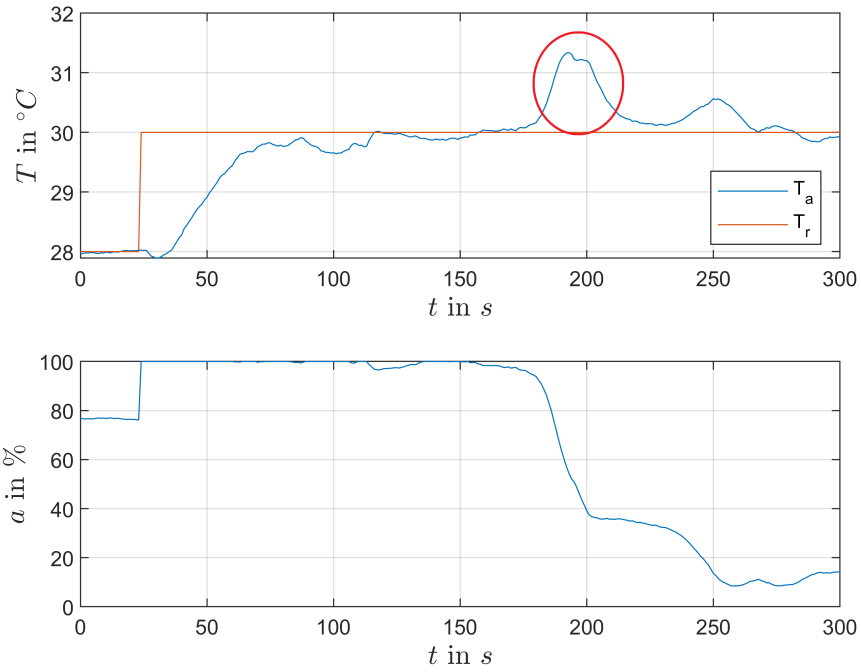

Figure 47: Measurement for the trapped air release error. The error is marked by the red circle.

6 Proband Tests

Proband tests were carried out to validate the adaptive climate control. The procedure of such a test is as follows:

Every test subject sits inside the car for about half an hour. The passenger of the car is asked to give feedback about his comfort every five minutes. Feedback is requested six times. The feedback consists of three variables, one for the head, one for the chest and one for the feet area. One variable can have an integer value ranging from -2 to 2, where the value is direct proportional to the thermal comfort in this area. A feedback of -2 means the thermal feeling in this area is cold, a feedback of 0 means the area is comfortable and a value of 2 means the area feels warm. A total of 15 proband tests were made. The room temperature was set on about $32°C$ to simulate outdoor summer climate conditions.

6.1 Control Analysis

One random proband test is picked for the examination of the developed control structure. The results of the temperature and the volume flow control are shown in Figure 48.

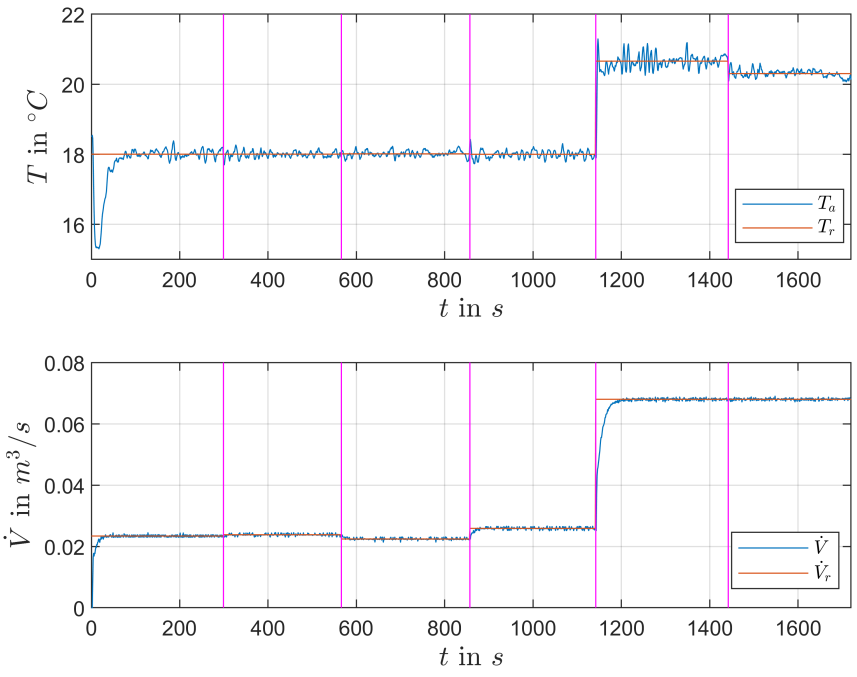

Figure 48: Proband test control results. The vertical lines represent the times of the feedback.

The overall result seems to be acceptable. The temperature oscillates the most at the time between $1200s$ and $1400s$. Since the feeling of temperature of the human body

does not react to such fast changes, the oscillations do not matter as long as the mean value is correct. The mean value of the temperature for the time from $1200s$ to $1400s$ is calculated and equals $\bar{T} = 20.66$. The reference temperature in that time step also equals $T_r = 20.66$.

This measurement also shows, that the control is able to compensate the hysteresis of the chiller.

For a better analysis, a closer look at the step response before the $1200s$ mark is taken. This step response is shown in Figure 49.

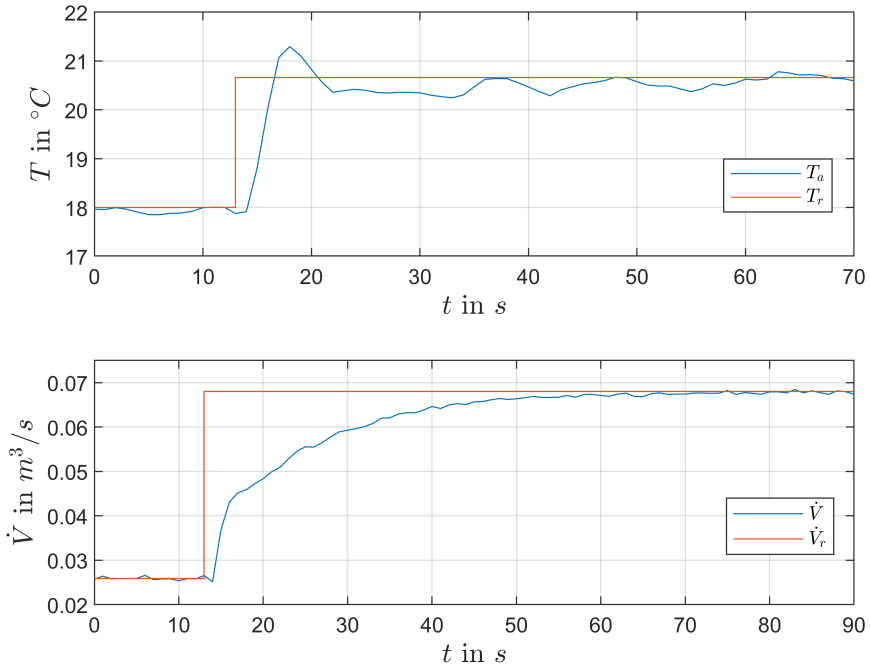

Figure 49: Step responses during the proband tests.

The temperature reacts sufficiently fast, but oscillates a bit around the reference signal. As stated above, these oscillations are no problem in this application. The volume flow could be faster with a higher sampling rate or a more aggressive controller, but since this control easily satisfies the requirements, no changes were made.

6.2 Validation of Comfort based HVAC Control

A quick overview of the first proband testing results is given here. To evaluate the results for the passenger comfort, the sum of the absolute values for the three areas were computed for the six feedback. That means, that a low value equals a high comfort. The results are shown in Figure 50. From time zero to the first feedback, the control was set at a calculated optimal comfort value for the given conditions. For this reason, the comfort for the first feedback is that good. After that, the comfort tends to diverge, especially for the feet area.

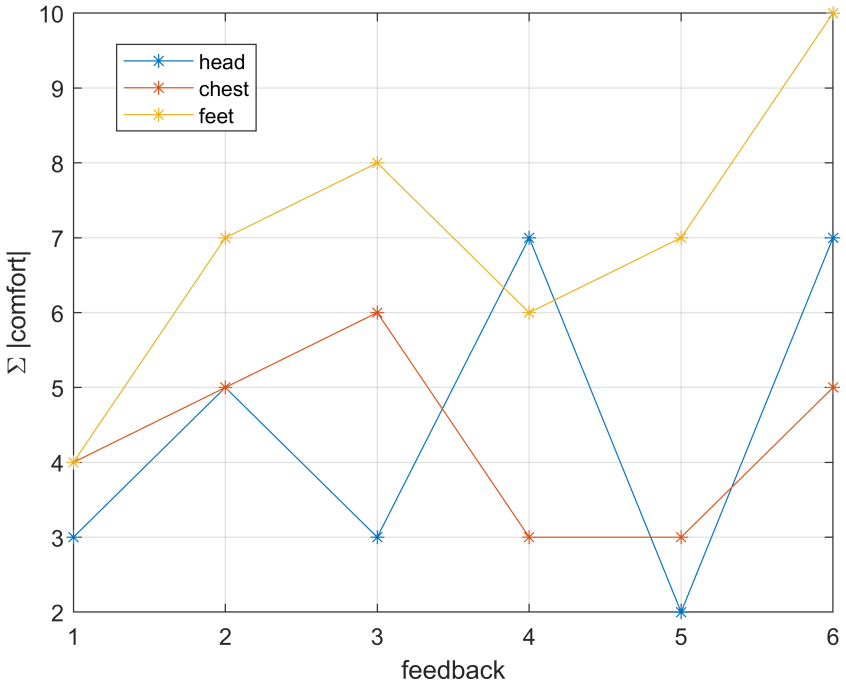

Figure 50: Sum of the absolute value for the three areas for every feedback.

The results are further analysed to find the cause of this diverging behavior. A histogram of the reference temperature and the reference volume flow given by the adaptive control for all references is computed. The results are shown in Figure 51. It is to note, that there is a total of seven reference signals for every test. Six feedbacks and one starting reference signal at time zero.

Starting with the volume flow, a good variation on the lower values can be observed. The highest bar, with 34 occurrences, includes the starting value and is, for this reason, so high. There are just a few values over $130m^3/h$ at about $240m^3/h$. It is unlikely to reach a high comfort with a high volume flow, since that would bother most passengers, for this reason, the results are plausible.

Now the histogram of the temperature is analysed. The values are either around 15, 18 or around 20, there is no in between. This really low variation of the temperature is for sure one reason for the increasing discomfort of the passengers.

Next, the consequences of a change in the feedback on the actuating signal are examined. The sum of the change in the feedbacks is computed on the abscissa, the resulting change in the control signal is shown on the ordinate of Figure 52. A high change of the feedback in the positive direction means the passengers feel warm in general. This should result in a fall of the temperature. As the measurement shows, the temperature does not really react.

The air temperature inside the car is always higher than the air entering the car. That means that a higher volume flow can take away more heat. The volume flow should increase when the change in feedback is positive. The trend of the measurements goes

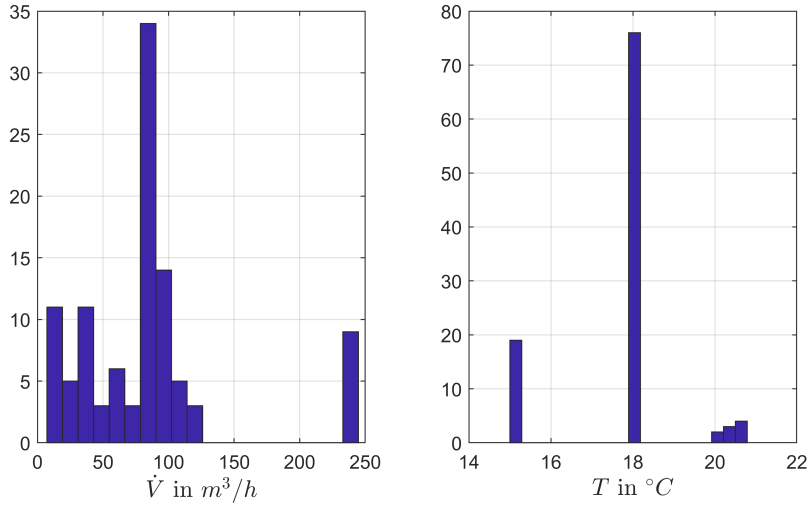

Figure 51: Histogram for the reference volume flow on the left and the reference temperature on the right.

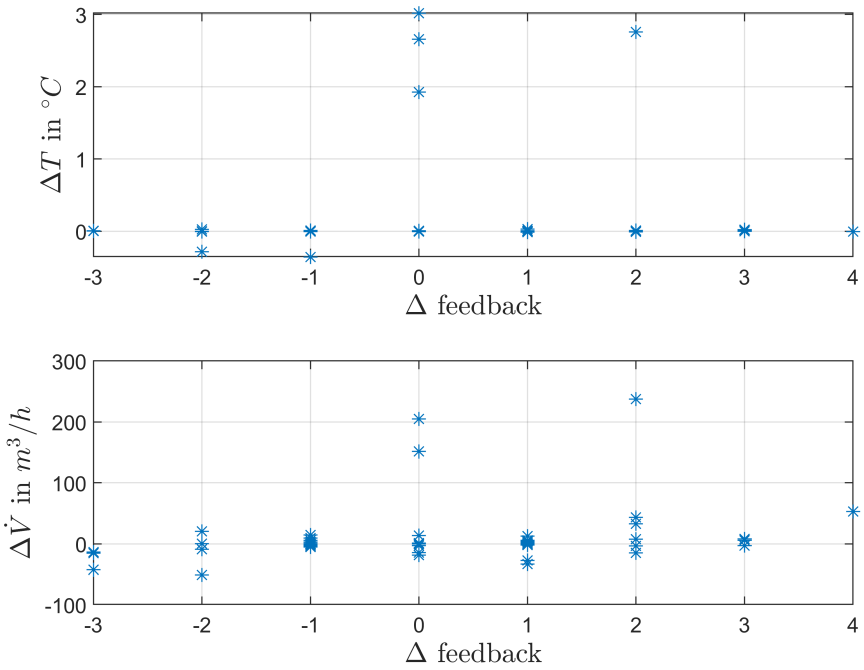

Figure 52: Change of the feedback on the abscissa and the resulting change of the reference signals on the ordinate.

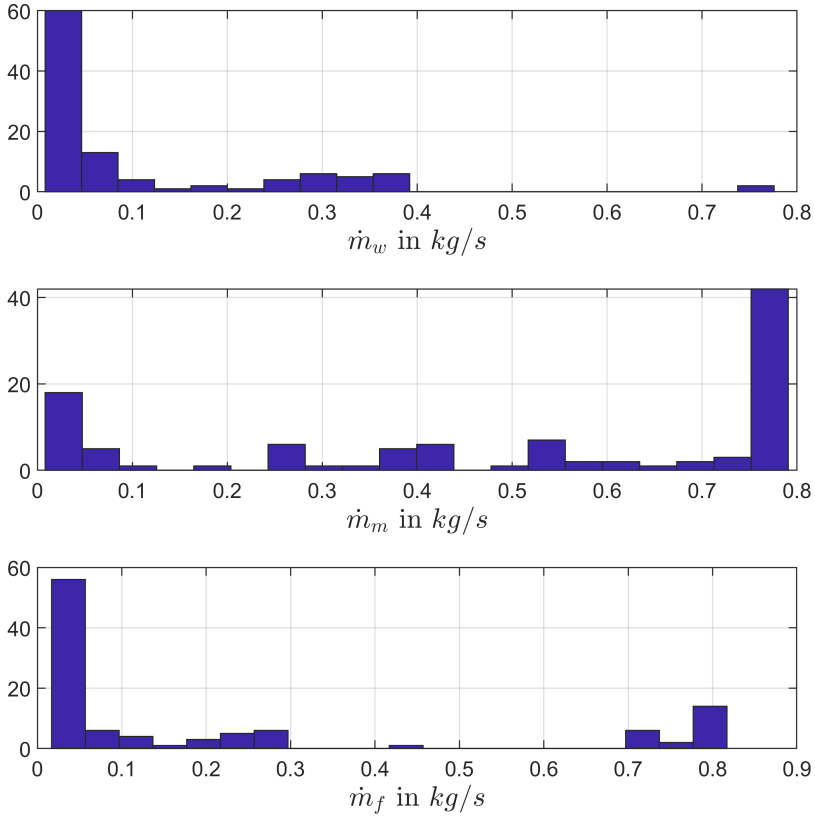

Figure 53: Normalized histogram of the reference mass flows at the outlet.

upwards, this looks plausible.

Next, the distribution of the air on the three outlets are considered. For that purpose, the mass flow at every area is divided with the total mass flow. This normalized mass flows are independent of the total mass flow. A histogram for every outlet is shown in Figure 53. As the three histograms show, most of the air enters the cabin from the middle inlet. The measurements simulated summer conditions, for this reason, it makes sense that most of the air enters trough the middle console, because the middle console directs the air to the chest and to the head. The chest and the head make up the majority of the body area, it is therefore reasonable, that those parts need more cooling. The mass flow leading to the windshield might cool the head a bit as well, but only slightly, since its main purpose is still the defrosting of the windshield. Also the mass flow leading to the feet is quite low most of the time. This might be reasonable, since the feet tend to be the coldest part of the body and will, for this reason, require less cooling.

At last we take a look at the reaction of the mass flow distribution to the feedback. Just like in Figure 52, the response of the adaptive control to the feedback is analyzed. As discussed above, the volume flow trough the middle inlets leads to the chest and

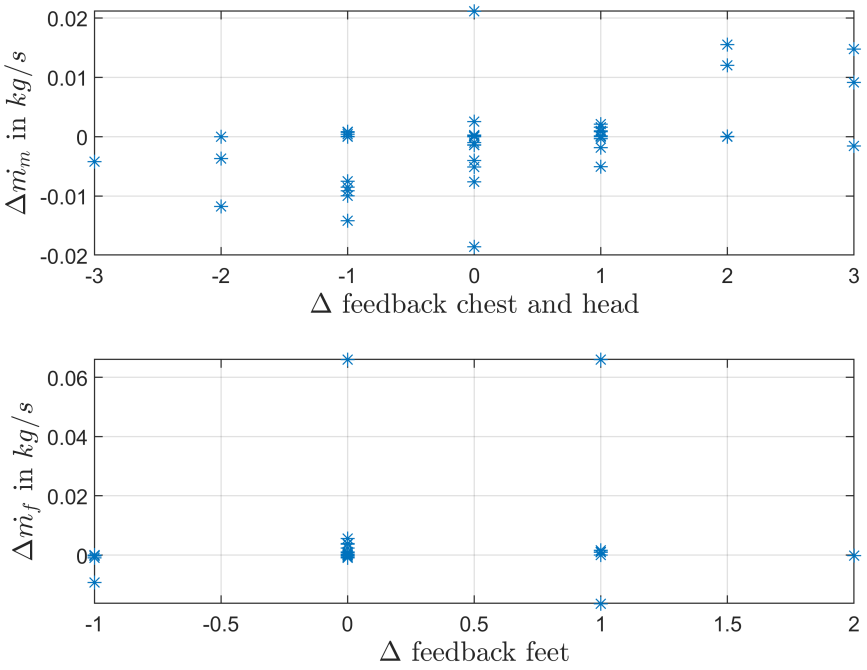

Figure 54: Change of the feedback on the abscissa and the resulting change of the mass flows on the ordinate.

head area, for this reason the two feedback values for head and chest are summed up. The result is shown in Figure 54. A rising trend on the middle inlet can be observed. Thinking logically, the trend should lead upwards, because a greater mass flow is able to take away more heat. The results are reasonable. The feedback on the feet seems to be uncorrelated to the resulting change of mass flow to the feet, this might be a systematic error.

This concludes the analysis of the preliminary proband tests. Most of the result seem plausible on a logical basis. A larger variation of the resulting reference signals probably leads to better results, that is especially true for the temperature.

7 Conclusions and possible Extensions

In this thesis, the HVAC-system of a driving simulator was automated. The main strategy is based on an adaptive comfort control. The focus of this work however, was placed on the modeling and control of the real vehicle environment.

The HVAC-system of the car was not designed to be automated, for this reason, the actuators, especially the temperature valve, are not really suited for the task. Furthermore, it is hard to make measurements, since the HVAC-box is not easily accessible. This made the modeling and the design of a controller more challenging.

Despite that, a simple control strategy has shown to yield good results for the volume flow control.

Also the temperature could be controlled using a PID-control. In this case, the control has shown to be less accurate. The use of a feedforward control could improve the results by lowering the oscillations, but no such control was used in this work, since the results were already satisfactory.

The air distribution on the single inlets has shown to be the most challenging problem. The validation measurements for the control strategy have a mediocre accuracy, for this reason, the results of the control still have a quite high degree of uncertainty.

It is hard to get much better results on this system. A test bench designed especially for this purpose would yield much better results and decrease the uncertainty of the measurements by a lot. Further possible improvements include independent temperature control for every inlet, automated control of the cabin air inflow direction. The position of the air inlets could be worth a discussion as well.

The first proband tests of the adaptive comfort control has shown, that the project leads in the right direction, but there are still a lot of improvements to do.

References

[1] Hans Dieter Baehr and Stephan Kabelac. *Thermodynamik: Grundlagen und technische Anwendungen ; mit zahlreichen Tabellen sowie 76 Beispielen*. 13., neu bearb. und erw. Aufl. Springer-Lehrbuch. Berlin: Springer, 2006. ISBN: 3-540-32513-1 (cit. on p. 14).

[2] Michael Bradley Bauer and Leighton Ira Davis JR. "Method and system for controlling an automotive HVAC system based on the principle of HVAC work". Pat. US5988517 (A). 1999 (cit. on p. 1).

[3] David R. Lide. "CRC Handbook of Chemistry and Physics, 84th Edition, 2003-2004". In: (), pp. 804, 974 (cit. on p. 28).

[4] Ronald D. Freiberger, Peter A. Thayer, and Diane M. Wills. "Adaptive climate control system". Pat. US5511724 (A). 1996 (cit. on p. 1).

[5] Frank Fusco and Gerhard A. Dage. "Adaptive controller for an automotive HVAC system". Pat. US6454178 (B1). 2002 (cit. on p. 1).

[6] Isaak Evseevič Idel'čik et al. *Handbook of hydraulic resistance*. 3rd ed., 6th Jaico impr. Mumbai [etc.]: Jaico Publishing House, 2008, p. 2 (cit. on p. 16).

[7] Jakob Fuchsberger. *Design of full variable HVAC Control*. Graz, 2021 (cit. on pp. 6, 13).

[8] Lev M. Klyatis. *Trends in Development of Accelerated Testing for Automotive and Aerospace Engineering*. Academic Press, 2020. ISBN: 978-0-12-818841-5 (cit. on p. 1).

[9] Möller Sebastian. *VIRTUAL VEHICLE Research GmbH*. Graz, 2021 (cit. on pp. 2, 3).

[10] Jonathan Stoia and Christopher Berthelet. "INFOTAINMENT SYSTEM WITH AIR-VENT CONTROL". Pat. WO2018106351 (A1). 2018 (cit. on p. 1).